Global study of separable pairing interaction in covariant density functional theory

S. Teeti and A. V. Afanasjev
Department of Physics and Astronomy, Mississippi State University, Mississippi 39762, USA

(Received 10 February 2021; accepted 1 March 2021; published 11 March 2021)

A systematic global investigation of pairing properties based on all available experimental data on pairing indicators has been performed for the first time in the framework of covariant density functional theory. It is based on the separable pairing interaction of Tian, Ma, and Ring [Phys. Lett. B **676**, 44 (2009)]. The optimization of the scaling factors of this interaction to experimental data clearly reveals its isospin dependence in the neutron subsystem. However, the situation is less certain in the proton subsystem since similar accuracy of the description of pairing indicators can be achieved both with isospin-dependent and mass-dependent scaling factors. The differences in the functional dependencies of scaling factors lead to uncertainties in the prediction of proton and neutron pairing properties which are especially pronounced at high isospin and could have a significant impact on some physical observables. For a given part of the nuclear chart the scaling factors for spherical nuclei are smaller than those for deformed ones; this feature exists also in nonrelativistic density functional theories. Its origin is traced back to particle-vibration coupling in odd-A nuclei which is missing in all existing global studies of pairing. Although the present investigation is based on the NL5(E) covariant energy density functional (CEDF), its general conclusions are expected to be valid also for other CEDFs built at the Hartree level.

DOI: 10.1103/PhysRevC.103.034310

I. INTRODUCTION

Pairing correlations play an extremely important role in nuclear physics: the inclusion of pairing [particle-particle (pp)] correlations is critical for open shell nuclei, and this is an absolute majority of the nuclei in the nuclear chart (see Refs. [1–3]). In principle the effective pp interaction is isospin dependent with isoscalar ($T = 0$) and isovector ($T = 1$) parts. However, only the isovector part is important since (i) the vast majority of pairing effects emerge from this part (see Refs. [1–3]) and (ii) there is no clear indications that the pp interaction in the $T = 0$ channel is strong enough to produce a pairing condensate (see Refs. [4,5]). That is a reason why we consider only isovector pairing interaction between like particles in the present paper.

It is well known that the pairing correlations play a significant role in the description of the ground state properties of open-shell nuclei. However, the properties of rotating nuclei and fission barriers are especially sensitive to fine details of pairing interaction. For example, the experimental moments of inertia of low and medium spin rotational bands and their evolution with spin cannot be described without inclusion of pairing interaction [3,6]. In addition, the accuracy of their description sensitively depends both on the details of pairing interaction [such as its form (for example, quadrupole pairing [7]) and strength (see Refs. [8–10])] and on (at least, approximate) particle number projection (such as Lipkin-Nogami method) (see Refs. [7–9,11,12]). The same situation exists also in the description of fission barriers. It was found in Ref. [13] that the pairing gap changes considerably with deformation and that relativistic mean field (RMF)+BCS calculations with constant gap do not provide an adequate description of the barriers. Relativistic Hartree-Bogoliubov (RHB) calculations show that there is a substantial difference in the predicted barrier heights between zero-range and finite-range pairing forces even in the case when the pairing strengths of these two forces are adjusted to the same value of the pairing gap at the ground state (see Ref. [13]). For zero range forces the barrier heights depend on the renormalization procedure. Note also that the details of pairing are important for the description of transitional nuclei since the modification of the strength of pairing could drive the system from transitional in nature to spherical, and vice versa (see the discussion of octupole deformed nuclei in Sec. V of Ref. [14]).

The pairing correlations are an important building block of different density functional theories (DFTs). Among these nuclear DFT's, covariant density functional theory (CDFT) is one of most attractive since covariant energy density functionals (CEDFs) exploit basic properties of QCD at low energies, such as symmetries and the separation of scales [15]. They provide a consistent treatment of the spin degrees of freedom, and they include the complicated interplay between the large Lorentz scalar and vector self-energies induced on the QCD level by the in-medium changes of the scalar and vector quark condensates [16]. In addition, these functionals include *nuclear magnetism* [17], i.e., a consistent description of currents and time-odd mean fields important for odd-mass nuclei [18], the excitations with unsaturated spins, magnetic moments [19], and nuclear rotations [20,21]. Because of Lorentz invariance no new adjustable parameters are required for the time-odd parts of the mean fields [18]. Of course,

at present, all attempts to derive these functionals, defining the particle-hole channel of the DFTs, directly from the bare forces [22–25] do not reach the required accuracy. Note that the same situation exists also in the nonrelativistic DFTs based on zero-range Skyrme and finite-range Gogny interactions (see Refs. [26,27] and references quoted therein). However, in recent years modern phenomenological CEDFs have been constructed [28–32] which provide an excellent description of ground and excited states all over the nuclear chart [33–37] with a high predictive power.

The pairing correlations and pairing indicators have been subjects of a number of studies within the framework of density functional theories (DFTs). For example, it was shown in Ref. [38] using Skyrme DFT that odd-even staggering (OES) of binding energies in light atomic nuclei is strongly affected by both nucleonic pairing and deformed mean field. Various approximations in the extraction of pairing indicators as well as in the calculations of pairing gaps in Skyrme DFT and their comparison with experimental data were investigated in Ref. [39]. The global analysis of pairing interaction was performed with the SLy4 functional and contact pairing interaction with possible density dependence employing different approximations such as the BCS, Hartree-Fock-Bogoliubov (HFB), and HFB with approximate particle number projection by means of the Lipkin-Nogami method in Ref. [40]. Other interesting results on pairing properties obtained in Skyrme DFT can be found in Refs. [41–45]. The mass dependence of the average pairing gap values for neutrons and protons was investigated in large scale Gogny DFT calculations with the Gogny D1S functional in Ref. [46]. However, this analysis is based on the comparison of experimental $\Delta^{(3)}$ indicators, extracted from binding energies, with theoretical averaged pairing gaps calculated in even-even nuclei. This drawback was removed in Refs. [47,48], in which experimental and theoretical $\Delta^{(3)}$ indicators were directly compared in several isotope chains of spherical and deformed nuclei across the nuclear chart (see Ref. [47]) in calculations with the D1S Gogny force and in deformed actinides in calculations with the D1M force (see Ref. [48]). Note that global analysis of this kind is still absent in the Gogny DFT. Other publications on particular aspects of the pairing interaction based on the Gogny forces were recently reviewed in Ref. [49]. Note that only nonrelativistic studies are mentioned here since the detailed discussion of the pairing studies within the CDFT is presented below.

In the literature on nuclear DFT several types of effective pairing forces $V^{\rm pp}$ have been used. The most simple force is the seniority force of Kerman [3,50] with constant pairing matrix elements G. This force is widely used, but is has many limitations, e.g., correlations in pairs with higher angular momentum are neglected, the scattering between pairs with different shells is not constant in realistic forces, the coupling to the continuum is not properly taken into account, and the predictive power is limited. As an alternative a (contact) zero-range δ force is used in many calculations and it is frequently made density dependent to be more realistic (see, for example, Refs. [40,43–45]). However, it is well known that these forces have the problem that, for calculations in full space, the pairing gap shows an ultraviolet divergence for any given strength of the interaction (see the discussion in Ref. [13] and references quoted therein).

Thus the search for more realistic pairing led to the use of finite-range Gogny force in the pairing channel of DFTs. Gogny derived his energy functional from a finite range force of the Brink-Booker type, which allows one to avoid the complicated problem of pairing cutoff [51]. This is because the finite range guarantees that the force decreases as a function of the momentum transfer and the gap equation converges without any problems. This type of pairing based on the D1S Gogny functional [52,53] (further called the Gogny pairing) has been used in the CDFT framework in many applications related to the description of the ground state properties [33,37,54], rotating nuclei [9,10,55], fission barriers [13], the nuclei in the vicinity of the proton and neutron drip lines [33,56], etc. Note that the pairing itself is a nonrelativistic effect which affects only the occupation of the single-particle states in the vicinity of the Fermi level; the impact of the pairing field on the small components of the Dirac spinor can be neglected to a very good approximation [57].

However, the use of the Gogny pairing is computationally time and memory consuming. Thus, a separable pairing interaction of finite range was introduced as a simplification of the Gogny pairing by Tian *et al.* in Ref. [58]. Its matrix elements in r-space have the form

$$V(\boldsymbol{r}_1,\boldsymbol{r}_2,\boldsymbol{r}_1',\boldsymbol{r}_2') = -f\,G\delta(\boldsymbol{R}-\boldsymbol{R'})P(r)P(r')\tfrac{1}{2}(1-P^{\sigma}) \tag{1}$$

with $\boldsymbol{R}=(\boldsymbol{r}_1+\boldsymbol{r}_2)/2$ and $\boldsymbol{r}=\boldsymbol{r}_1-\boldsymbol{r}_2$ being the center-of-mass and relative coordinates. The form factor $P(r)$ is of Gaussian shape:

$$P(r)=\frac{1}{(4\pi a^2)^{3/2}}e^{-r^2/4a^2}. \tag{2}$$

The factor f is the scaling factor of the pairing force, which in general is particle number dependent, i.e., $f=f(Z,N)$ (see Ref. [36]). The parameters $G=728$ MeV fm^3 and $a=0.644$ fm of this interaction, which are the same for protons and neutrons, have been derived by a mapping of the $^1S_0$ pairing gap of infinite nuclear matter to that of the Gogny force D1S [58] under the condition that $f=1.0$. These parameters are also used in the present paper. In finite nuclei, the pairing gaps calculated with separable pairing interaction and Gogny pairing are very close to each other (see Ref. [36]). Because numerical calculations with separable pairing interaction are less time consuming that those with Gogny pairing, its use has become widespread in CDFT calculations of ground state properties [36,37,59,60], fission properties [61–63], the properties of rotating nuclei [64,65], and in many beyond mean field and QRPA calculations [66–69] based on the CDFT framework.

In many CDFT applications both the Gogny and separable pairing interactions have been used with scaling factor $f=1.0$. However, over the years it became clear that the pairing force based on the D1S force does not fully take into account the mass and particle dependencies of the experimental pairing. For the first time, this feature has been seen in the cranked relativistic Hartree-Bogoliubov (CRHB) calculations

of rotational properties of a few actinides in Ref. [70], and later it was confirmed in more systematic CRHB calculations of Ref. [10] in the same mass region. The analysis of odd-even staggering in nuclear binding energies of spherical nuclei has also revealed the need for mass or particle number dependencies of the Gogny D1S pairing for the reproduction of experimental pairing indicators [36,71]. These results indicate that the pairing effects are underestimated for light nuclei and overestimated for heavy ones when the Gogny D1S force is used in the pairing channel. A similar situation exists also for separable pairing interaction, the parameters of which are defined by the fit to the Gogny D1S force [36].

It is necessary to recognize that the studies of particle number dependencies of the Gogny and separable pairing in the CDFT framework have been performed either in localized regions of nuclear chart or for specific types of systems such as spherical nuclei in Refs. [36,71] or rotating nuclei in Refs. [10,70]. As a consequence, even nowadays these dependencies are neglected in many applications of the CDFT. Thus, the goal of the present paper is to perform for the first time a global study of separable pairing interaction in the CDFT framework and optimize its particle number dependencies.

The paper is organized as follows. Experimental pairing indicators are discussed in Sec. II. The discussion of theoretical pairing gaps is presented in Sec. III. Section IV is devoted to the analysis of the results of the calculations and optimization of pairing interaction. The extrapolation properties of optimized separable pairing towards very neutron-rich nuclei and related theoretical uncertainties are discussed in Sec. V. Finally, Sec. VI summarizes the results of our paper.

II. EXPERIMENTAL PAIRING INDICATORS

There are several expressions for the pairing indicators in the literature. These are three-, four-, and five-point indicators[1] given by

$$\Delta_i^{(3)}(Q_0) = \frac{\pi_{Q_0}}{2}[B(Q_0-1) - 2B(Q_0) + B(Q_0+1)], \quad (3)$$

$$\Delta_i^{(4)}(Q_0) = \frac{\pi_{Q_0}}{4}[B(Q_0-2) - 3B(Q_0-1) + 3B(Q_0) - B(Q_0+1)], \quad (4)$$

$$\Delta_i^{(5)}(Q_0) = -\frac{\pi_{Q_0}}{8}[B(Q_0+2) - 4B(Q_0+1) + 6B(Q_0) - 4B(Q_0-1) + B(Q_0-2)], \quad (5)$$

which quantify the OES of binding energies. Here Q_0 is equal to either proton (Z) or neutron (N) number, $\pi_{Q_0} = (-1)^{Q_0}$ is the number parity in the respective subsystem, and $B(Q)$ is the (negative) binding energy of a system with Q particles. In these equations, if the number of protons Z is fixed, then

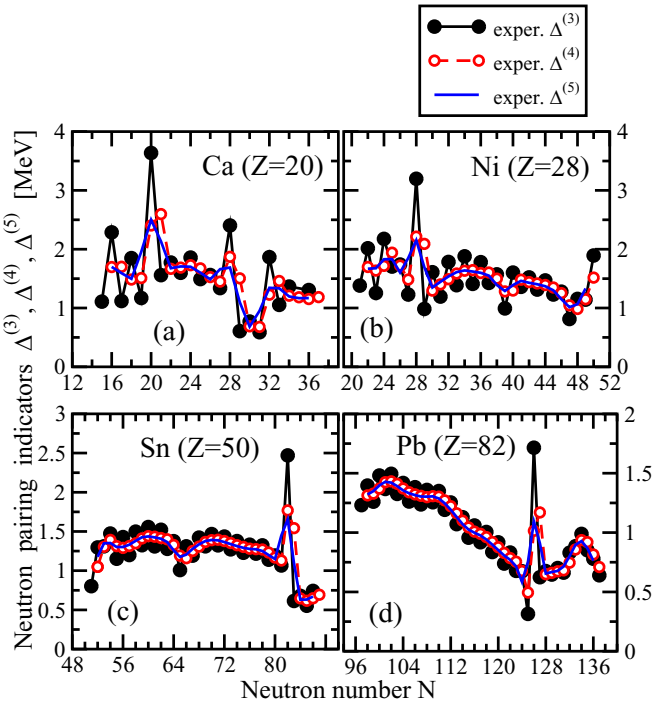

FIG. 1. Experimental neutron pairing indicators $\Delta_\nu^{(3)}(Z,N)$, $\Delta_\nu^{(4)}(Z,N)$, and $\Delta_\nu^{(5)}(Z,N)$ as a function of the neutron number N for indicated isotopic chains of spherical nuclei.

$i = \nu$ and the indicator gives the neutron OES. Otherwise, we obtain proton ($i = \pi$) OES if the number of neutrons is fixed. The number parity π_{Q_0} is chosen in such a way that the OES is positive irrespective of its centering at either even or odd particle number Q_0.

These experimental indicators are illustrated for spherical nuclei in Figs. 1 and 2. The $\Delta^{(3)}$ indicator shows a significant odd-even staggering. This staggering is washed out when the $\Delta^{(4)}$ and $\Delta^{(5)}$ indicators are used. The $\Delta^{(4)}$ indicator gives an expression which is asymmetric around the nucleus with Q_0 and therefore offers two choices [39]. Thus, we use in further studies the $\Delta^{(5)}$ indicator which is symmetric and expected to yield better decoupling from mean-field effects [39].

One should note that the peaks in these indicators (which are especially pronounced for the $\Delta^{(3)}$ ones) appear at $Q_{\rm shell}$ values corresponding to the shell closures or neighboring Q values. These are the peaks in neutron pairing indicators at $N = 20$ and $N = 28$ in the Ca isotopes, at $N = 28$ and $N = 50$ in the Ni isotopes, at $N = 50$ in the Sn isotopes, and at $N = 126$ in the Pb isotopes (see Fig. 1). Similar peaks are also seen in proton pairing indicators at $Z = 20$ in the $N = 20$ and $N = 28$ isotones, at $Z = 50$ in the $N = 82$ isotones, and $Z = 82$ in the $N = 126$ isotopes (see Fig. 2). These peaks in no way should be interpreted as an indication of increased pairing correlations. This is connected with the fact that pairing correlations either disappear or are significantly weakened at shell closures (see discussion in Sec. IV of Ref. [36]) and the peaks are not produced by pairing, but by the large or substantially increased shell gaps for closed-shell configurations. Therefore, proton/neutron $\Delta^{(5)}$ quantities corresponding to

[1]Note that these pairing indicators are derived from the Taylor expansion of the nuclear mass in nucleon-number differences [39]. As a result, they depend on a number of assumptions, some of which are strongly violated at shell closures (see the discussion in Sec. 4.2 of Ref. [39]).

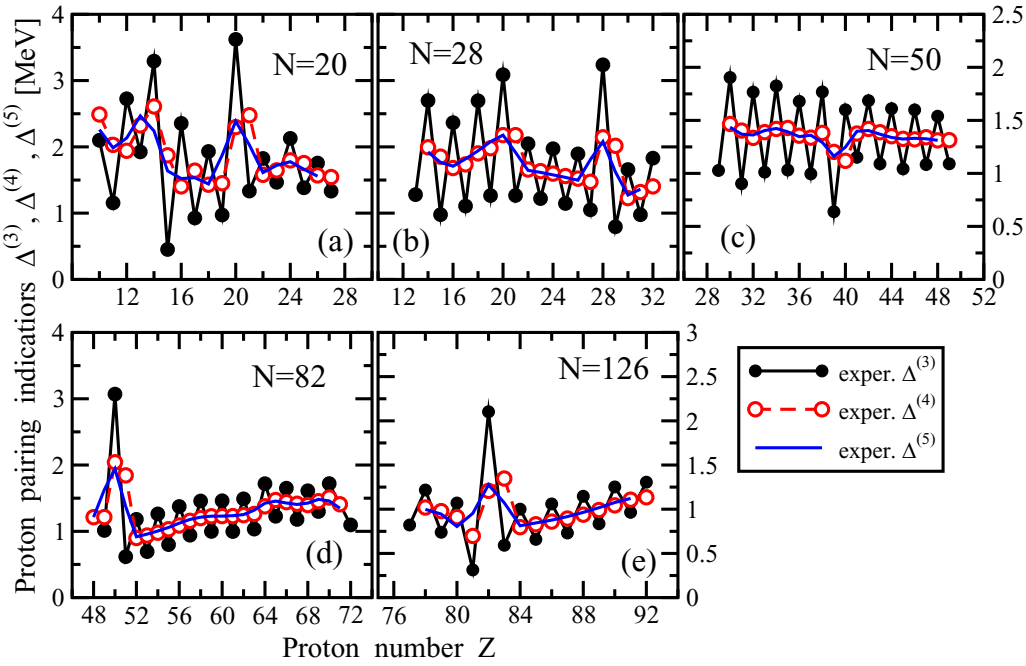

FIG. 2. The same as Fig. 1 but for proton indicators $\Delta_\pi^{(3)}(Z,N)$, $\Delta_\pi^{(4)}(Z,N)$, and $\Delta_\pi^{(5)}(Z,N)$ as a function of proton number Z for indicated isotonic chains of spherical nuclei.

such peaks at proton/neutron shell closures and their close vicinities do not represent pairing indicators and thus are eliminated from the consideration.

It is interesting to estimate global relative differences in the definition of experimental $\Delta^{(4)}$ and $\Delta^{(5)}$ indicators by means of the function

$$D_i = \frac{1}{n_i^{\rm set}} \sum_{Z,N} \frac{\left|\Delta_i^{(5)}(Z,N) - \Delta_i^{(4)}(Z,N)\right|}{\Delta_i^{(5)}(Z,N)} \times 100\%. \quad (6)$$

Here the sum runs over $n_i^{\rm set}$ nuclei for which pairing indicators are available and the subscript i indicates the subsystem (proton or neutron). The analysis of all available experimental data based on the AME2016 compilation of Ref. [72] (see, for example, Figs. 3 and 4 below and their discussion) leads to $D_\pi = 5.50\%$ and $D_\nu = 2.68\%$ if the pairing indicators at $Q = Q_{\rm shell}$ are excluded from consideration and to improved values of $D_\pi = 4.20\%$ and $D_\nu = 1.93\%$ if the pairing indicators at $Q = Q_{\rm shell}, Q_{\rm shell} \pm 2$ are excluded from consideration. These numbers suggest that, even on the level of experimental data, the pairing indicators suffer from some degree of uncertainty and are not uniquely defined.

It is necessary to recognize that all these definitions of the OES of the binding energies do not provide a clean measure of pairing correlations since they have contributions which are not directly related to them. These include

(1) Non-negligible contributions in time-even and time-odd mean fields from the response of the underlying mean field to the blocking of a single-particle state in odd-mass nuclei [18,38,39,73]. This includes also the effects from the breaking of Kramer's degeneracy of the single-particle states in odd-A nuclei [18].

(2) The impact of the fact that the structure (in terms of the Nilsson orbital) of the experimental ground states in odd-A nuclei is reproduced globally only in approximately 40% of the nuclei in the DFTs [74,75].[2] As a consequence, the impact of the blocked orbital on the deformations and binding energies of the ground state is expected to deviate somewhat (see, for example, Fig. 4 in Ref. [75] for deformation effects) from that expected for the case when the ground state is based on the single-particle orbital with correct structure. These facts are ignored in an absolute majority of the studies of pairing via OES of binding energies. It is only in Ref. [47] that this feature has been mentioned, but the suggested recipe (not used by the authors of Ref. [47] themselves), namely, the use of binding energy of the one-quasiparticle configuration with correct Nilsson structure in the calculations of OES, suffers from substantial uncertainties in the description of the energies of the single-particle states in the DFT frameworks [48,76].

(3) The impact of (quasi)particle-vibrational coupling on the binding energies of odd-mass nuclei. This impact is especially pronounced in spherical nuclei [76,77].[3] According to the quasiparticle-phonon model

[2]The inclusion of particle-vibrational coupling increases the accuracy of the description of the single-particle configurations in odd-A nuclei but such studies are limited to spherical nuclei (see Refs. [76,77]).

[3]It is interesting that such features have already been mentioned in seminal article of Dechargé and Gogny [78] where they indicated

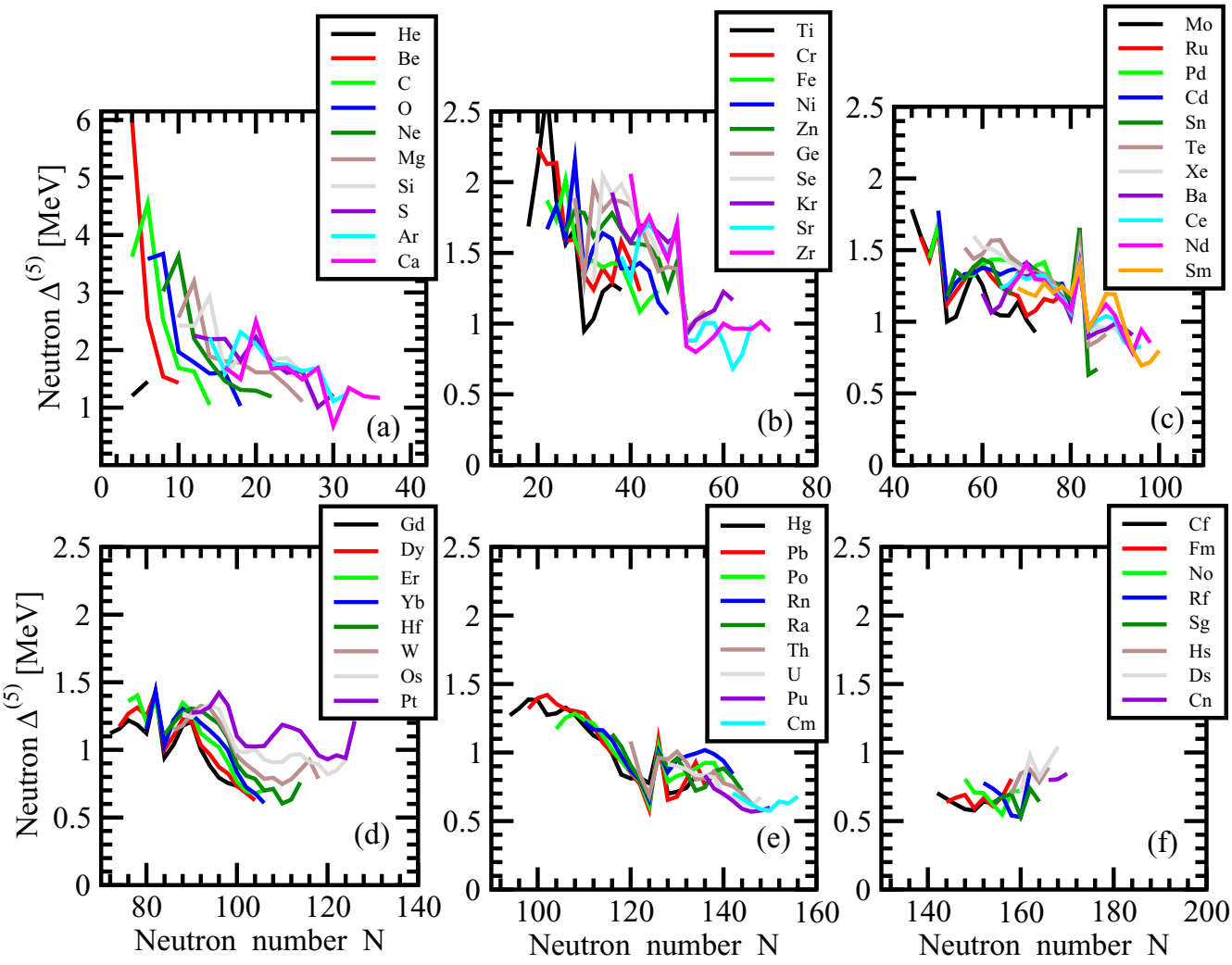

FIG. 3. Experimental neutron $\Delta_v^{(5)}(Z,N)$ indicators as a function of neutron number N. Pairing indicators based both on measured and estimated binding energies (see discussion in the beginning of Sec. IV) are included. The data are grouped into six panels according to increasing proton number. This is done to illustrate both the isospin dependence and the impact of different shell closures on the $\Delta_v^{(5)}(Z,N)$ indicators. The ranges of the neutron number and $\Delta_v^{(5)}(Z,N)$ changes are the same in panels (b)–(f); this allows direct comparison of the slopes of the $\Delta_v^{(5)}(Z,N)$ values as a function of neutron number in these panels. Note that these ranges are different in panel (a). The experimental data on binding energies are taken from the AME2016 mass evaluation (see Ref. [72]).

of Soloviev [2], the admixtures of the phonons to the structure of the ground states in deformed rare-earth and actinide odd-mass nuclei is relatively small (especially, when compared with spherical nuclei) [79–81].

(4) It was also found in Ref. [82] that the random-phase approximation based part of the total shell correction, which accounts for the neutron-proton pair-vibrational correlation energy, contributes significantly to the calculated odd-even mass differences, particularly in the light nuclei.

Thus, one can conclude that the comparison of experimental pairing indicators extracted from binding energies with theoretical results obtained from mean field type calculations can reveal only general trends of pairing evolution as a function of particle numbers, and local differences between theory and experiment are expected. One should also recognize that global investigations of pairing at the beyond mean field level are not possible nowadays. The analysis of pairing interaction at the mean field level based on experimental data which by definition includes beyond mean field effects suggest that the latter should be to a degree treated as a "noisy" data, where the noise is coming from neglected beyond mean field effects. As a consequence, special attention has to be paid to the reduction of the impact of the data which strongly deviate from general trends (for example, by employing robust fitting procedures (see Sec. IV below) as well as on the comparative analysis of

that treating explicitly the residual interaction through configuration mixing in odd and even nuclei is expected to lower the OES by approximately 300 keV in the Sn isotopes.

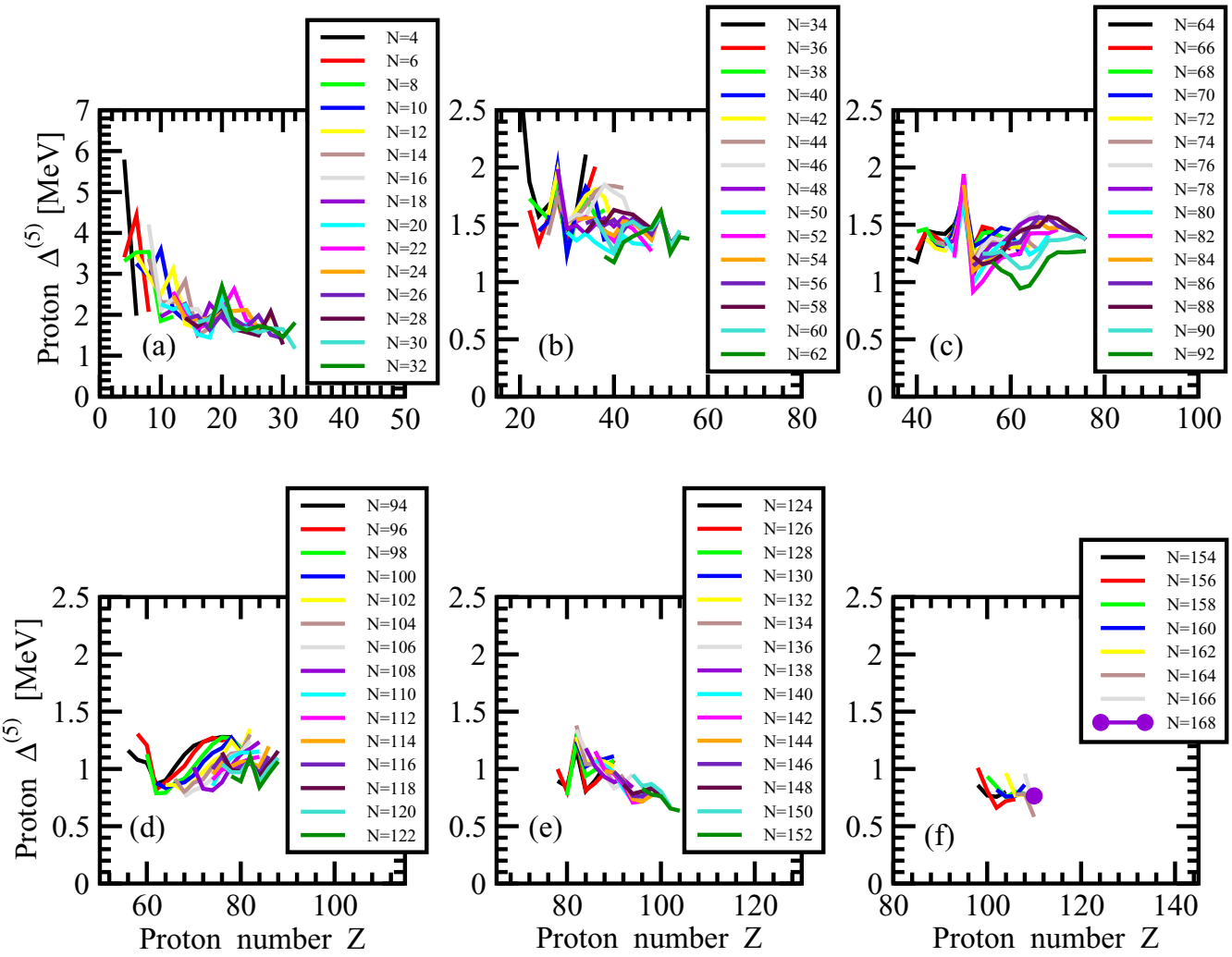

FIG. 4. The same as in Fig. 3 but for the proton $\Delta_\pi^{(5)}(Z,N)$ indicators as a function of proton number Z.

different types of nuclei and different regions of the nuclear chart.

III. THEORETICAL PAIRING GAPS

In the present paper, the relativistic Hartree-Bogoliubov (RHB) approach is used in the calculations. The formalism of this approach is discussed in detail in Refs. [33,36]. Thus, we consider here only technical details related to pairing interaction. Note that for this study we employ the NL5(E) [32] covariant energy density functional (CEDF) which globally outperforms well known NL3 [83] and NL3* [84] functionals (see Ref. [32]).

The pair field $\hat{\Delta}$ in the RHB theory is given by

$$\hat{\Delta} \equiv \Delta_{n_1 n_2} = \frac{1}{2}\sum_{n_1' n_2'} \langle n_1 n_2 | V^{\rm pp} | n_1' n_2' \rangle \kappa_{n_1' n_2'}. \tag{7}$$

It contains the pairing tensor κ,

$$\kappa = V^* U^T, \tag{8}$$

and the effective interaction $V^{\rm pp}$ in the particle-particle channel for which the separable pairing interaction of Eq. (1) is used. In theoretical calculations we use pairing gap[4]

$$\Delta_{\rm uv} = \frac{\sum_k u_k v_k \Delta_k}{\sum_k u_k v_k}, \tag{9}$$

which provides a better description of experimental pairing indicators in the CDFT framework as compared with other forms of pairing gaps (see Sec. IV in Ref. [36]).

For each even-even nucleus under consideration we define neutron and proton scaling factors $f_\nu(Z,N)$ and $f_\pi(Z,N)$ of

[4]The pairing gap $\Delta_{\rm uv}$ is related to the average of the state dependent gaps over the pairing tensor. $\Delta_{\rm uv}$ averages over $u_k v_k$, a quantity which is concentrated around the Fermi surface. However, because of the fact that $\kappa \sim \sum_k u_k v_k$ diverges for the seniority force and for zero range forces, $\Delta_{\rm uv}$ turns out to depend on the pairing window. This is, however, no problem for the separable pairing of finite range used in this investigation.

separable pairing force [see Eq. (1)] from the condition

$$\Delta^{i}_{\rm uv}(Z,N) = \Delta^{(5)}_{i-cor}(Z,N), \tag{10}$$

where $\Delta^{(5)}_{i\text{-cor}}(Z,N)$ (defined below) stands for the experimental $\Delta^{(5)}(Z,N)$ pairing indicator corrected for the effects of time-odd mean fields in odd-A nuclei. Here subscript i indicates the subsystem (proton or neutron). This is done for all even-even (Z,N) nuclei for which either the experimental $\Delta^{(5)}_{\nu}(Z,N)$ indicator or the experimental $\Delta^{(5)}_{\pi}(Z,N)$ indicator or both of them are available.

The $\Delta^{(5)}_{\nu\text{-cor}}$ and $\Delta^{(5)}_{\pi\text{-cor}}$ indicators are determined by means of Eq. (5) but with experimental binding energies of odd nuclei $B^{\text{odd-}i}(Z,N)$ corrected for the impact of time-odd mean fields (ΔE_i) via

$$B^{\text{odd-}i}_{cor}(Z,N) = B^{\text{odd-}i}(Z,N) + \Delta E_i. \tag{11}$$

This is equivalent to averaged removal of time-odd effects from odd-A nuclei and allows us to compare the $\Delta^{(5)}_{\nu\text{-cor}}$ and $\Delta^{(5)}_{\pi\text{-cor}}$ indicators with the respective calculated $\Delta_{\rm uv}$ pairing gaps which do not include time-odd mean fields. Note that this leads to slight increase of the $\Delta^{(5)}_{\nu\text{-cor}}$ and $\Delta^{(5)}_{\pi\text{-cor}}$ values as compared with the $\Delta^{(5)}_{\nu}$ and $\Delta^{(5)}_{\pi}$ ones.

The need for such a correction comes from the fact that time-odd mean fields (nuclear magnetism in the CDFT framework; see Refs. [18,85]) provide an additional binding in odd-Z and odd-N nuclei but have no effect on binding energies of even-even nuclei (see Ref. [18]). As a consequence, respective pairing indicators defined by Eqs. (3), (4), and (5) will be modified (see also Sec. III D in Ref. [18] and Ref. [86]).

Note that additional bindings due to time-odd mean fields only weakly depend on CEDF [18]. Thus, we use averaged functions ΔE_N and ΔE_Z for additional bindings in odd-N and odd-Z nuclei due to time-odd mean fields as defined for the NL3 functional in Ref. [18], namely,

$$\begin{aligned} \Delta E_\nu &= 0.73 N^{-0.58}\ [\text{MeV}], \\ \Delta E_\pi &= 0.37 Z^{-0.54}\ [\text{MeV}]. \end{aligned} \tag{12}$$

The powers of these expressions are similar for different subsystems. On the other hand, the magnitudes in front of the base of power differ considerably between proton and neutron quantities, indicating weaker additional binding due to time-odd mean fields for odd-proton nuclei.

The analysis based on the use of the $\Delta^{i}_{uv}(Z,N)$ pairing gaps has the advantage that these quantities are calculated in even-even nuclei. This allows one to avoid the complicated problem of calculating the blocked states in odd-mass nuclei (see Refs. [10,75] and the discussion below). On the other hand, the validity of their use in the comparison with experimental $\Delta^{(5)}_{i}(Z,N)$ indicators is not obvious. It turns out, however, that away from spherical shell closures, the $\Delta^{i}_{\rm uv}(Z,N)$ values come close to the calculated $\Delta^{(5)}_{i}(Z,N)$ indicators [36]. To verify that for the chains of spherical nuclei shown in Figs. 1 and 2 we compared the $\Delta^{(5)}_{i}(Z,N)$ indicators, obtained in the calculations without time-odd mean fields, with calculated $\Delta^{i}_{uv}(Z,N)$ pairing gaps. In both types of calculations the Gogny D1S force was used in the pairing channel. This analysis is very similar to the one presented in Sec. IV of Ref. [36] but performed without time-odd mean fields in odd-A nuclei. It turns out that the average deviation between $\Delta^{(5)}_{i}(Z,N)$ and $\Delta_{uv}(Z,N)$ quantities for this set of nuclei is on the level of approximately 5% if shell closure nuclei with $Q_{\rm shell}$ and their neighbors with $Q_{\rm shell} \pm 2$ are excluded from consideration. However, the proton and neutron scaling factors have to be modified on average by only $\approx$2% to compensate for this difference between the two quantities. This value defines the accuracy of the approach and it is sufficient for the analysis of global trends.

An alternative to the above described procedure would be fully self-consistent calculations of binding energies of even-even and odd-mass nuclei with the inclusion of the effects of time-odd mean fields and blocking in odd-A nuclei. It would lead to theoretical $\Delta^{(5)}_{i}(Z,N)$ (or lower order) indicators defined by Eq. (5) [Eqs. (3) and (4)] which can directly be compared with experimental ones. Such an approach has been employed for isotopic (with magic Z) and isotonic (with magic N) chains of spherical nuclei and the set of deformed actinides calculated with triaxial RHB computer code with fixed scaling factors $f_\nu(Z,N)$ and $f_\nu(Z,N)$ in Refs. [10,36]. However, this alternative procedure has its own disadvantages. First of all, systematic calculations within the CDFT [75] and non-relativistic Skyrme DFT [74] showed that in more than half of odd-A nuclei the single-particle structure of the ground states cannot be reproduced. This means that the polarization effects in time-even (deformation) and time-odd channels affecting the binding energies are not properly defined in these odd-A nuclei. Second, the effects of particle-vibration coupling will modify the binding energies of odd-A nuclei; this effect is expected to be especially pronounced in spherical systems (see Ref. [76]). Third, the definition of the ground state in a given deformed odd-A nucleus requires the blocking of approximately ten lowest in energy quasiparticle states [75]; a somewhat smaller number of the states is needed to be considered in spherical nuclei [36,39]. Numerical calculations of the blocked solutions in odd-A nuclei are appreciably more time consuming than the ones without blocking in even-even nuclei. In addition, there are problems with the convergence of such blocked solutions for some configurations [10,48,75]. Finally, global calculations using this procedure with the optimization of scaling factors $f_\nu(Z,N)$ and $f_\pi(Z,N)$ are prohibitively time consuming.

IV. DISCUSSION

The binding energies given in the AME2016 mass evaluation [72] can be separated into two groups: one represents the nuclei with binding energies defined only from experimental data, the other contains the nuclei with binding energies depending in addition on either interpolation or extrapolation procedures. As a consequence, there are the $\Delta^{(5)}_{i}(Z,N)$ indicators which are defined only by experimentally measured binding energies and the $\Delta^{(5)}_{i}(Z,N)$ indicators which in addition depend on estimated binding energies. For simplicity, we call the $\Delta^{(5)}_{i}(Z,N)$ indicators (and related scaling factors) in the first and second groups as "measured" and "estimated." Based on the binding ener-

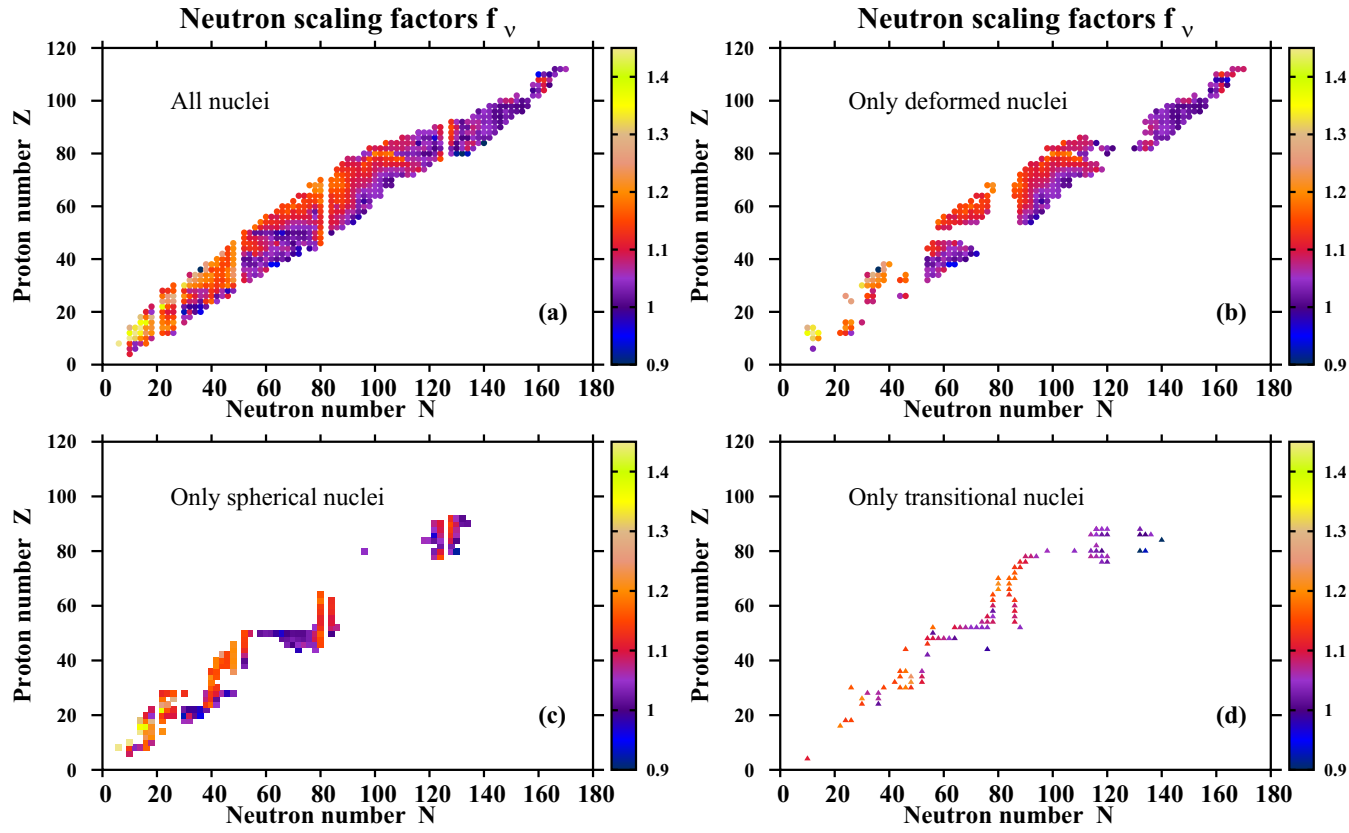

FIG. 5. The distribution of the scaling factors $f_\nu(Z,N)$ of neutron pairing in the nuclear chart. Panel (a) shows all nuclei for which experimental $\Delta_\nu^{(5)}(Z,N)$ indicators can be defined. Note, however, that we exclude such indicators for $N = 20$, 50, 82, and 126. Panels (b), (c), and (d) show scaling factors only for the nuclei whose ground states are either deformed, spherical, or transitional according to the calculations. The nuclei with equilibrium deformations β_2 satisfying the conditions $|\beta_2| \leqslant 0.02$, $0.02 < |\beta_2| < 0.15$, and $|\beta_2| \geqslant 0.15$ are considered to be spherical, transitional, and deformed, respectively.

gies available in AME2016 evaluation one can define 612 neutron and 611 proton measured $\Delta_i^{(5)}(Z,N)$ indicators and 110 neutron and 53 proton estimated $\Delta_i^{(5)}(Z,N)$ indicators. Altogether, there are 722 and 664 proton and neutron "measured+estimated" $\Delta_i^{(5)}(Z,N)$ indicators. Note that we consider only even-even and odd nuclei in this paper since the binding energies of odd-odd nuclei are affected by the residual neutron-proton interaction of an unpaired proton and neutron.

Experimental neutron and proton $\Delta_i^{(5)}(Z,N)$ pairing indicators are shown in Figs. 3 and 4 for different isotopic and isotonic chains, respectively. The analysis of these figures reveals the following general features. First, there is a substantial staggering of these indicators as a function of respective particle numbers which is especially visible in light nuclei and at spherical shell closures. Large peaks appear in the experimental $\Delta_i^{(5)}(Z,N)$ indicators at spherical shell closures. In no way they should be considered as indication of increased pairing: this is connected with the fact that pairing correlations either disappear or are extremely weak in closed shell nuclei in theoretical calculations. These peaks are not produced by pairing, but by increased shell gap for closed-shell configurations. Second, there is a general trend of the reduction neutron/proton $\Delta_i^{(5)}(Z,N)$ pairing indicators with increasing proton/neutron numbers. Third, on average neutron $\Delta_\nu^{(5)}(Z,N)$ indicators for a given isotope chain decrease with increasing neutron number (or equivalently isospin) (see Fig. 3). This trend is disturbed at spherical shell closures, which is especially visible at $N = 50$ in Fig. 3(b), at $N = 50$ and $N = 82$ in Fig. 3(c), and at $N = 126$ in Figs. 3(d) and 3(e). Only actinides and light superheavy nuclei do not show this trend [see Fig. 3(f)] but this feature is most likely due to the presence of large deformed $N = 162$ shell gap (see Ref. [87]) which leads to an increase of the $\Delta_\nu^{(5)}(Z,N)$ values in its vicinity. This fact may also indicate that some fluctuations in pairing indicators of lighter nuclei are also due to deformed shell gaps. Fourth, if one excludes light nuclei, proton pairing indicators show more constant (on average) proton $\Delta_\pi^{(5)}(Z,N)$ indicators for a given isotonic chain as a function of proton number as compared with neutron $\Delta_\pi^{(5)}(Z,N)$ indicators for a given isotopic chain as a function of neutron number (compare Figs. 4 and 3). Again this trend is disturbed at spherical shell closures, which is visible as the peaks in $\Delta_\pi^{(5)}(Z,N)$, especially at $Z = 28$ in Fig. 4(b), at $Z = 50$ in Fig. 4(c), and at $Z = 82$ in Fig. 4(e).

Neutron and proton scaling factors $f_\nu(Z,N)$ and $f_\pi(Z,N)$ defined from the condition of Eq. (10) are presented in Figs. 5 and 6. These figures reveal several general trends. First, the scaling factors in both subsystems decrease with increasing

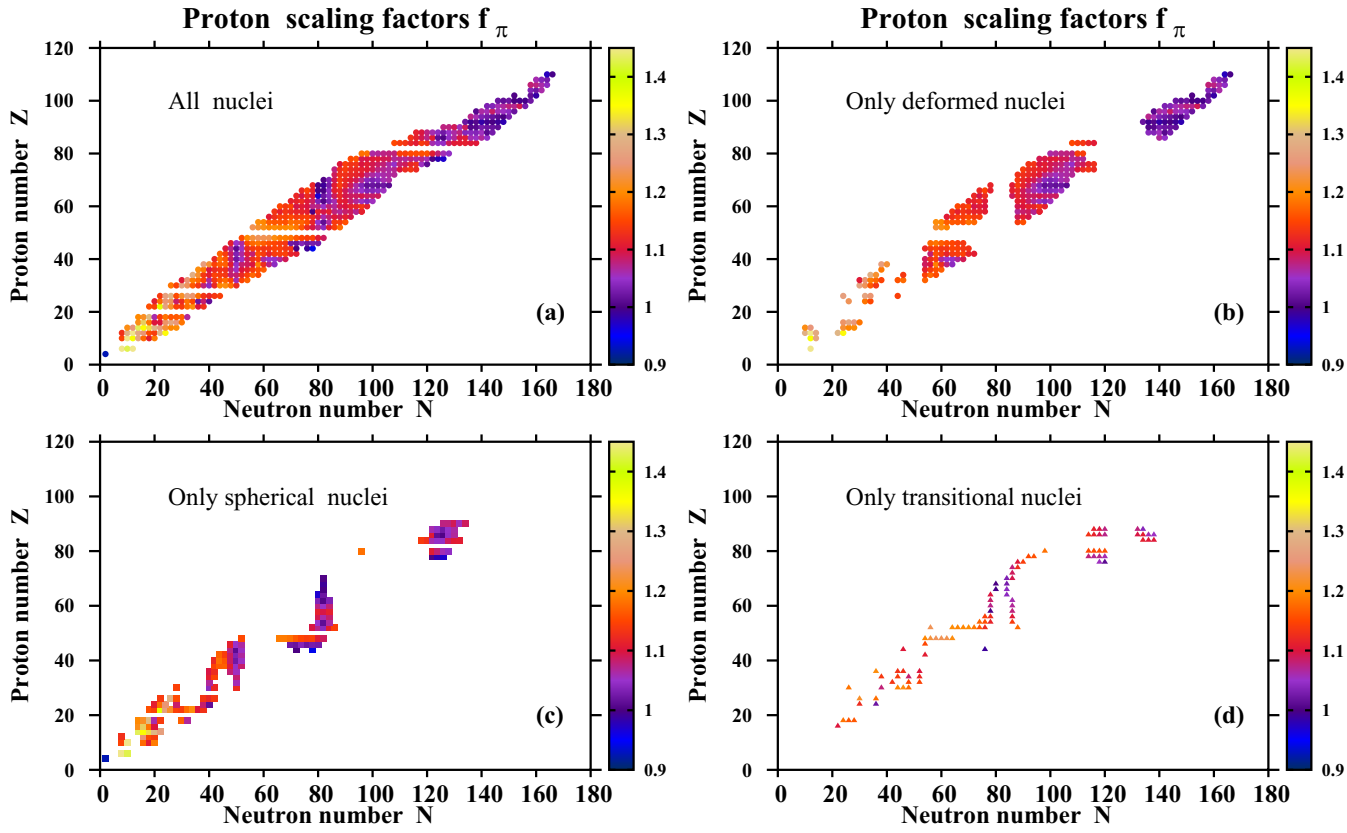

FIG. 6. The same as Fig. 5 but for proton scaling factors $f_\pi(Z,N)$ of proton pairing. Note, however, that we exclude proton pairing indicators for $Z = 20$, 50, and 82.

mass number. Second, neutron scaling factors $f_\nu(Z,N)$ also decrease with increasing isospin [see Fig. 5(a)]. However, this trend is less pronounced in proton subsystem [see Fig. 6(a)]. Third, in a given part of nuclear chart the scaling factors for spherical nuclei are smaller than those for deformed ones.[5] This is clearly seen for neutron scaling factors $f_\nu(Z,N)$ near proton shell closures at $Z = 20$, 28, and 50 [see Figs. 5(a) and 5(c)] and for proton scaling factors near neutron shell closures at $N = 50$, 82, and 126 [see Figs. 5(a) and 5(c)]. The comparisons of Figs. 5(b) and 5(c) for the neutron subsystem and Figs. 6(b) and 5(c) for the proton subsystem also reveal this feature. The origin of this feature could be related to the impact of particle-vibration coupling (PVC) impact on the binding energies of odd-mass nuclei. The PVC increases the binding energies of odd-A nuclei (see Ref. [76,78]) and thus reduces the pairing indicators. Its effect is more pronounced in spherical nuclei as compared with deformed ones and thus in a given region of nuclear chart it leads to a suppression of scaling factors in spherical nuclei as compared with the ones in deformed nuclei. An alternative possible explanation of the difference in pairing strength in spherical and deformed nuclei is related to the differences in the single-particle densities in the vicinity of the Fermi levels of such nuclei (see Sec. IV of Ref. [40]). However, in general this effect should be taken into account already at the mean field level with proper treatment of pairing correlations.

It is interesting to see whether the approximate global functional dependences of scaling factors can be defined and which form of such dependences provides the best description of extracted scaling factors on a global scale. For that we have investigated the functionals dependencies[6]

$$f_\pi(Z,N) = C_\pi A^{\alpha_\pi}, \qquad f_\nu(Z,N) = C_\nu A^{\alpha_\nu}, \tag{13}$$

$$f_\pi(Z,N) = C_\pi Z^{\alpha_\pi}, \qquad f_\nu(Z,N) = C_\nu N^{\alpha_\nu}, \tag{14}$$

[5]Note that the analysis within the Skyrme DFT with zero-range density-dependent pairing interaction also reveals that pairing interaction extracted from OES of binding energies is smaller in spherical nuclei as compared with that in deformed ones [40]. The results of the Gogny DFT calculations for a few isotope chains of spherical and deformed nuclei presented in Ref. [47] reveal a similar situation: the strength of pairing interaction as defined by the D1M Gogny forces has to be decreased/increased in spherical/deformed nuclei in order to reproduce experimental $\Delta^{(3)}$ indicators.

[6]We also investigated functional dependencies of the $f_i(Z,N) = C_i e^{\alpha_i N} e^{\beta_i Z}$ and $f_i(Z,N) = C_i e^{\alpha_i [N/(N+Z)]} e^{\beta_i [Z/(N+Z)]}$ $(i = \pi, \nu)$ types which depend on three parameters: C_i, α_i, and β_i. These expressions represent the generalization of Eqs. (16) and (17) which depend on two parameters. However, the addition of a third parameter improves the goodness of fit only marginally as compared with that obtained with two parameters in Table I and thus does not offer substantial benefits in the light of existing limitations of the method. As a consequence, they are not considered in further discussion.

TABLE I. The parameters of global functional dependencies (see text for details) defined by the fits to the sets of "measured+estimated" and "measured" scaling factors. The standard nonlinear least squares fitting is employed here. The bold style is used for RMSE of the best fit in each group of functional dependencies.

	Measured+estimated			Measured		
	C_i	α_i	RMSE	C_i	α_i	RMSE
1	2	3	4	5	6	7
$f_\pi = C_\pi A^{\alpha_\pi}$	1.529	−0.0672	**0.0549**	1.528	−0.0669	**0.0550**
$f_\pi = C_\pi Z^{\alpha_\pi}$	1.455	−0.0695	0.0554	1.455	−0.0690	0.05536
$f_\pi = C_\pi \lvert N-Z\rvert^{\alpha_\pi}$	1.256	−0.04367	0.0567	1.256	−0.0433	0.0569
$f_\pi = C_\pi e^{\alpha_\pi \lvert N-Z\rvert}$	1.176	−0.0025	0.0566	1.178	−0.00259	0.0569
$f_\pi = C_\pi e^{\alpha_\pi [\lvert N-Z\rvert/(N+Z)]}$	1.156	−0.264	0.0685	1.154	−0.244	0.0685
$f_\nu = C_\nu A^{\alpha_\nu}$	1.388	−0.0503	0.0614	1.404	−0.0524	0.0592
$f_\nu = C_\nu N^{\alpha_\nu}$	1.369	−0.0536	0.0594	1.382	−0.0554	0.0572
$f_\nu = C_\nu \lvert N-Z\rvert^{\alpha_\nu}$	1.249	−0.0471	**0.0529**	1.253	−0.0478	**0.0511**
$f_\nu = C_\nu e^{\alpha_\nu \lvert N-Z\rvert}$	1.154	−0.0024	0.0561	1.159	−0.00255	0.0548
$f_\nu = C_\nu e^{\alpha_\nu [\lvert N-Z\rvert/(N+Z)]}$	1.192	−0.551	0.0577	1.191	−0.535	0.0578

$$f_\pi(Z,N) = C_\pi |N-Z|^{\alpha_\pi}, \quad f_\nu(Z,N) = C_\nu |N-Z|^{\alpha_\nu}, \tag{15}$$

$$f_\pi(Z,N) = C_\pi e^{\alpha_\pi |N-Z|}, \quad f_\nu(Z,N) = C_\nu e^{\alpha_\nu |N-Z|}, \tag{16}$$

$$f_\pi(Z,N) = C_\pi e^{\alpha_\pi \frac{|N-Z|}{N+Z}}, \quad f_\nu(Z,N) = C_\nu e^{\alpha_\nu \frac{|N-Z|}{N+Z}} \tag{17}$$

in order to see whether mass, particle number, and isospin dependencies can be disentangled. Here the indices π and ν stands for proton and neutron quantities, respectively. Separate scaling factors for proton and neutron subsystems reflect explicit breaking of the isospin symmetry in the pairing energy functional, which is standard in nearly all pairing forces (see, for example, Refs. [39,40,88]).

The functional dependencies given by Eqs. (13)–(17) are determined by means of nonlinear least-squares fitting to the set of proton and neutron scaling factors presented in Figs. 5 and 6. Note that we eliminate from this data set the scaling factors for $N = Z$ since they show enhanced values as compared with neighboring nuclei [see Figs. 5(a) and 6(a)]. This enhancement is due to Wigner energy which affects both binding energies of the $N = Z$ nuclei and related pairing indicators. These features are also a reason why in functional dependencies including isospin we use $|N-Z|$ instead of $(N-Z)$. However, only a few scaling factors are available for light nuclei on the proton-rich side of the $N = Z$ line [see Figs. 5(a) and 6(a)] for which $(N-Z) < 0$. Thus, in general, the impact of modulus in $|N-Z|$ on the quality of the fit is expected to be small.

The fitting is performed by Curve Fitting Toolbox™ software of MATLAB. The goodness of fit is defined by root mean squared error (RMSE). The main disadvantage of least squares fitting is its sensitivity to outliers. Outliers can have a large influence on the fit because squaring the residuals magnifies the effects of these extreme data points. Thus, in addition to standard nonlinear least squares fitting we also employ robust nonlinear least squares fitting with bisquare width regression scheme. This scheme minimizes a weighted sum of squares, where the weight given to each data point depends on how far the point is from the fitted line. The points located near the line get full weight and the points farther from the line obtain reduced weight. The points that are farther from the line than would be expected by random chance get zero weight.

The results of these fits are presented in Tables I, II, and III. One can see that the parameters and the goodnesses of fit depend very little on whether "measured+estimated" or only "measured" scaling factors are used (see Table I). The RMSEs are almost the same in the proton subsystem for the fits to both sets of data but in the neutron subsystem they slightly increase when going on from the fit to only "measured" scaling factors to the fit which includes "measured+estimated" ones. Thus, in the following discussion we will consider only the fits to "measured+estimated" scaling factors in order to have access to the larger set of data with high isospin.

For the proton subsystem, the best fit is obtained for functional dependence of Eq. (13) (see Table I). Figure 7(a) compares the distribution of scaling factors as a function of mass number A with a fitted curve. They both show a general

TABLE II. The same as Table I but for the case of robust nonlinear least square fitting based on the bisquare width regression scheme. Note that only "measured+estimated" scaling factors are used in the fit. The RMSEs from column 4 of the Table I are shown in column 5 [labeled as RMSE(A)].

	C_i	α_i	RMSE	RMSE(A)
1	2	3	4	5
$f_\pi = C_\pi A^{\alpha_\pi}$	1.555	−0.0706	0.0515	**0.0549**
$f_\pi = C_\pi Z^{\alpha_\pi}$	1.471	−0.0722	0.0529	0.0554
$f_\pi = C_\pi \lvert N-Z\rvert^{\alpha_\pi}$	1.248	−0.0421	0.0513	0.0567
$f_\pi = C_\pi e^{\alpha_\pi \lvert N-Z\rvert}$	1.169	−0.00235	**0.0491**	0.0566
$f_\pi = C_\pi e^{\alpha_\pi [\lvert N-Z\rvert/(N+Z)]}$	1.167	−0.358	0.0596	0.0685
$f_\nu = C_\nu A^{\alpha_\nu}$	1.36	−0.0462	0.0598	0.0614
$f_\nu = C_\nu N^{\alpha_\nu}$	1.355	−0.0511	0.0582	0.0594
$f_\nu = C_\nu \lvert N-Z\rvert^{\alpha_\nu}$	1.24	−0.0446	0.0501	**0.0529**
$f_\nu = C_\nu e^{\alpha_\nu \lvert N-Z\rvert}$	1.147	−0.00216	0.0521	0.0561
$f_\nu = C_\nu e^{\alpha_\nu [\lvert N-Z\rvert/(N+Z)]}$	1.19	−0.573	**0.0485**	0.0577

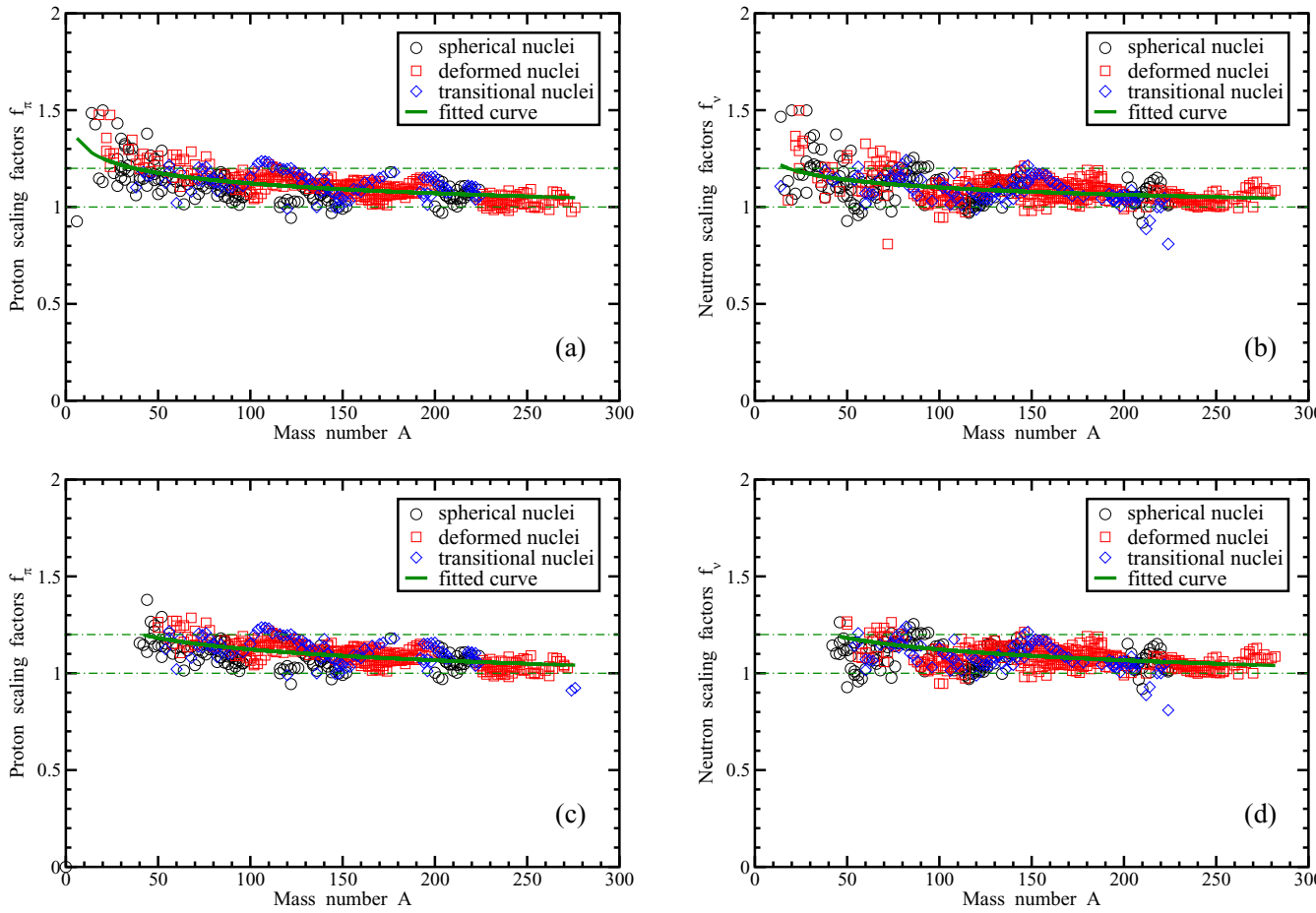

FIG. 7. Proton $[f_\pi(Z,N)]$ and neutron $[f_\nu(Z,N)]$ scaling factors as a function of mass number A. Open circles, squares, and diamonds are used for spherical, transitional, and deformed nuclei, respectively. Top panels include all available scaling factors, while bottom panels show only those for the nuclei with $Z > 20, N > 20$. Solid green lines correspond to global functional dependencies given by Eqs. (13) with the parameters from Table I for top panels and from Table III for bottom panels.

trend of the decrease of scaling factors with increasing mass number. In addition, the oscillations of the scaling factors, averaged for a given range of A, with respect to the fitted curve as a function of mass number are clearly visible, especially for spherical and transitional nuclei. The largest spread of scaling factors from fitted curves are seen for the light nuclei. This is not surprising considering the fact that these nuclei are soft in deformation degrees of freedom so that the correlations beyond mean field are expected to play an enhanced role in their structure. For this reason also the quality of mass description in light nuclei in the CDFT is also lower than in medium and heavy mass regions (see Ref. [36]). Comparable to Eq. (13), goodness of fit is obtained also with functional dependencies given by Eqs. (14), (15), and (16) (see Table I). The quality of the fit and the spreads of scaling factors with respect of the fitted curve are illustrated by the example of the functional dependence of $f_\pi(Z,N) = C_\pi e^{\alpha_\pi |N-Z|}$ type in Fig. 8. There is a general trend of the decrease of the fitted f_π curve and individual scaling factors with the increase of isospin factor $|N-Z|$. The largest spread of the scaling factors with respect of the fitted curve is observed at low isospin. The worst fit of proton scaling factors is provided by the functional dependence of Eq. (17) (see Table I) and Fig. 9(a)).

It is interesting to see how these conclusions will be modified if the least reliable data points are excluded from consideration. These are typically the points (outliers) which

TABLE III. The same as Table II but for the case when light nuclei with $N < 20$ and $Z < 20$ are excluded from consideration. The RMSEs from column 4 of the Table II are shown in column 5 [labeled as RMSE(B)).

1	C 2	α 3	RMSE 4	RMSE(B) 5
$f_\pi = C_\pi A^{\alpha_\pi}$	1.578	−0.0739	0.0496	0.0515
$f_\pi = C_\pi Z^{\alpha_\pi}$	1.458	−0.0699	0.0504	0.0529
$f_\pi = C_\pi \lvert N-Z\rvert^{\alpha_\pi}$	1.242	−0.0406	0.0502	0.0501
$f_\pi = C_\pi e^{\alpha_\pi \lvert N-Z\rvert}$	1.165	−0.00226	**0.0476**	**0.0491**
$f_\pi = C_\pi e^{\alpha_\pi [\lvert N-Z\rvert/(N+Z)]}$	1.163	−0.353	0.0564	0.0596
$f_\nu = C_\nu A^{\alpha_\nu}$	1.360	−0.0462	0.0574	0.0598
$f_\nu = C_\nu N^{\alpha_\nu}$	1.355	−0.0510	0.0557	0.0582
$f_\nu = C_\nu \lvert N-Z\rvert^{\alpha_\nu}$	1.237	−0.0438	0.0479	0.0501
$f_\nu = C_\nu e^{\alpha_\nu \lvert N-Z\rvert}$	1.145	−0.00212	0.0503	0.0521
$f_\nu = C_\nu e^{\alpha_\nu [\lvert N-Z\rvert/(N+Z)]}$	1.192	−0.595	**0.0462**	**0.0485**

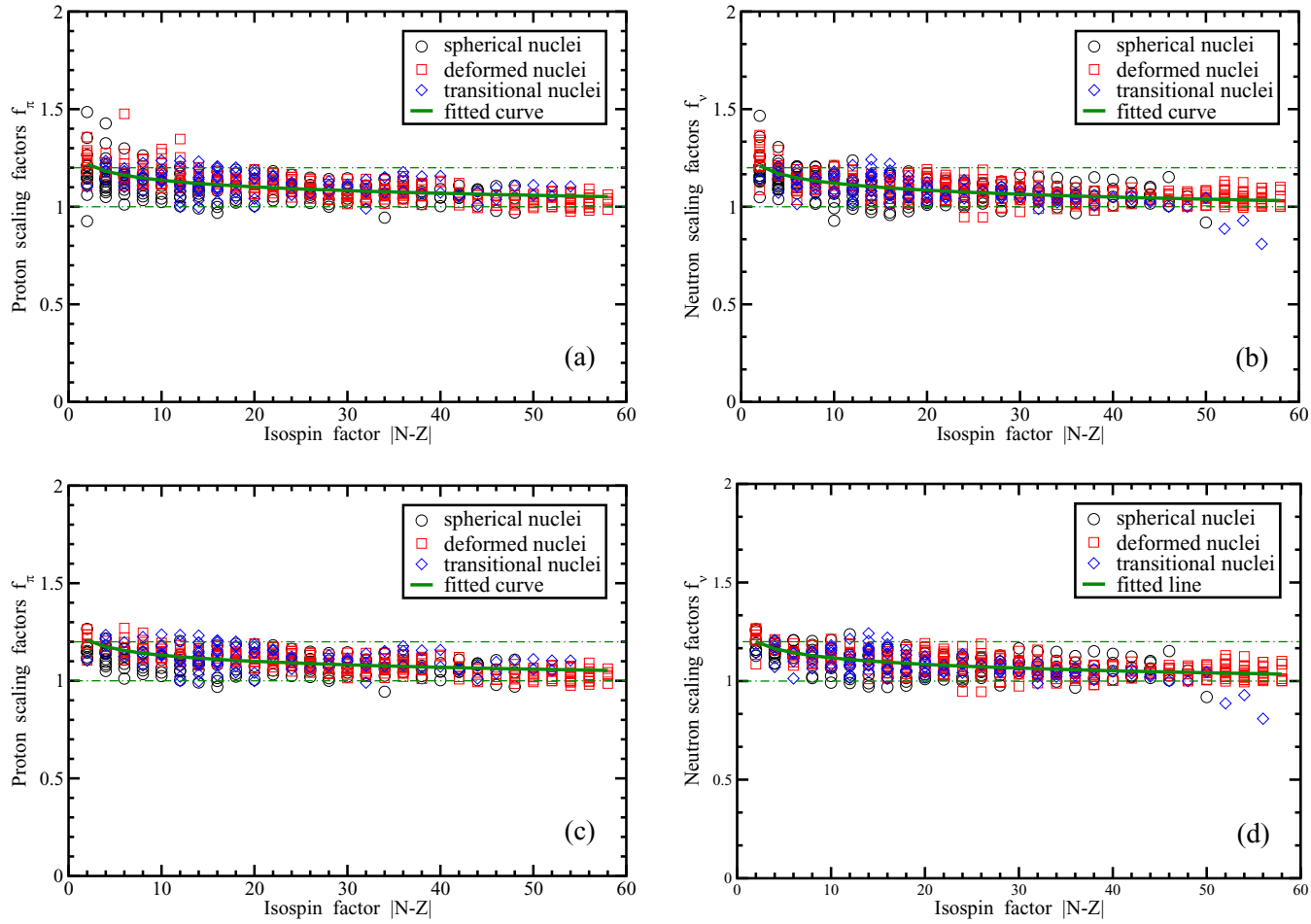

FIG. 8. The same as Fig. 7 but as a function of isospin factor $|N - Z|$. Solid green lines correspond to global functional dependencies given by Eqs. (15) with the parameters from Table I for top panels and from Table III for bottom panels.

are located far away from the fitted curve. They can be caused, for example, by the limitations of the mean field approximation and the neglect of beyond mean field effects. These effects are expected to be especially important in light nuclei or for the pairing indicators, the determination of which involves two types of the nuclei (for example, transitional and deformed ones). Table II shows how the RMSEs are modified when robust nonlinear least squares fitting based on the bisquare width regression scheme is used instead of the standard one. One can see that in all cases it improves RMSEs. The fitting protocol based on the $f_\pi(Z, N) = C_\pi e^{\alpha_\pi |N-Z|}$ functional dependence becomes the best, and is closely followed by the functional dependences of Eqs. (13), (14), and (16). The exclusion of light nuclei leads to further improvement in the RMSEs (see Table III) but does not modify the conclusions obtained based on the results of Table II. Figures 7(c), 8(c), and 9(c) compare fitted curves based on the parameters of Table III with the distribution of respective individual scaling factors. One can see that in all cases the number of outliers is decreasing drastically [as compared with Figs. 7(a), 8(a) and 9(a)] and the distribution of individual scaling factors becomes more condensed around the fitted curve.

Similar features have also been observed for the neutron subsystem. The majority of outliers are produced again by the light nuclei [compare Figs. 7(d), 8(d), and 9(d) with Figs. 7(b), 8(b), and 9(b)] and their removal leads to the improvement of goodness of fit (compare Tables II and III). Robust nonlinear least squares fitting based on the bisquare width regression scheme improves RMSEs in all fits as compared with the standard one (compare Tables I and II). However, the principal difference as compared with the proton subsystem is the fact that isospin dependence (in one or another form) of neutron scaling factors is substantially favored as compared with the mass or neutron number dependences given by Eqs. (13) and (14) in all fits. The best RMSEs are provided either by the $f_\nu(Z, N) = C_\nu |N - Z|^{\alpha_\nu}$ (Table I) or by the $f_\nu(Z, N) = C_\nu e^{\alpha_\nu \frac{|N-Z|}{N+Z}}$ (Tables II and III) functional dependencies. However, in the light of their closeness in terms of RMSEs and the approximations used in this study it is impossible to give a clear preference to one or another.

The present study clearly favors the functional dependencies of scaling factors (and, thus of pairing interaction) which depend on the isospin in neutron subsystem. The situation is more mixed in the case of the proton subsystem since functional dependencies of scaling factors on mass/particle numbers produce RMSEs which are only slightly above those produced by functional dependencies which include isospin.

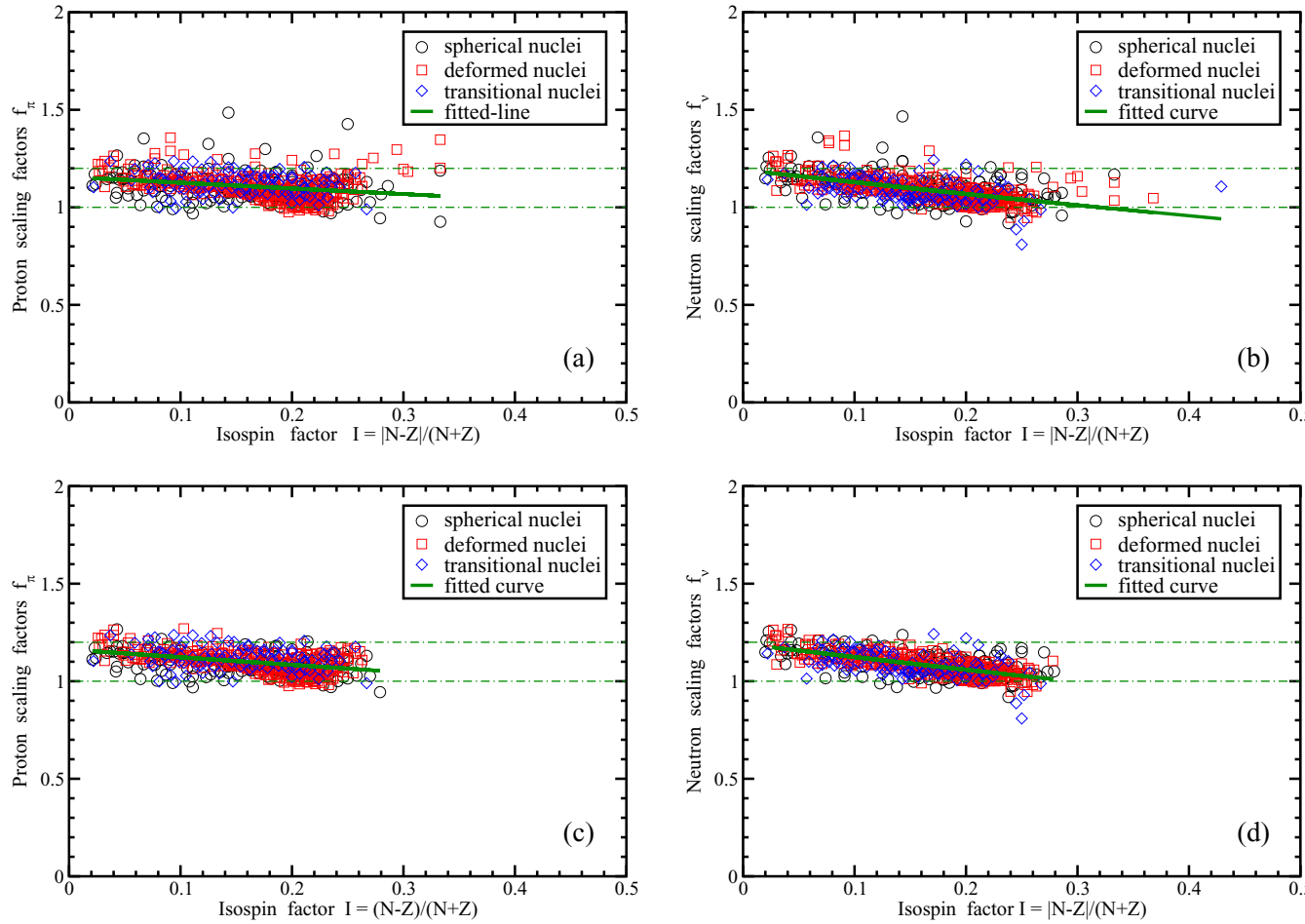

FIG. 9. The same as Fig. 7 but as a function of isospin factor $I = \frac{|N-Z|}{N+Z}$. Solid green lines correspond to global functional dependencies given by Eqs. (17) with the parameters from Table I for top panels and from Table III for bottom panels.

The origin of this feature is not completely clear. However, the possible origin could be related to the fact that the RPA neutron-proton pair-vibrational correlation energy is expected to decrease numerically with increasing neutron excess due to an increasing mismatch of the occupations of single-neutron and single-proton levels (see Ref. [82]). This could lead to more pronounced isospin dependence of neutron pairing as compared with the proton one.

To our knowledge, the isospin dependence of the Gogny pairing interaction in the Gogny DFT has not been studied so far. The isospin dependence of pairing interaction has been revealed by several global studies in the framework of Skyrme DFT (see Refs. [43,44]). However, it is necessary to point out that the isoscalar-density dependence used in these works is phenomenological and it is not motivated by any arguments based on the microscopic theory of effective interaction [44].

In the light of substantial differences in the scaling factors of spherical and deformed nuclei within the given region of the nuclear chart discussed above it is interesting to repeat the analysis but with the restriction to only scaling factors defined in deformed nuclei. The results of such analysis are summarized in Table IV. One can see that the exclusion of spherical and transitional nuclei from the fitting leads to a substantial improvement in RMSEs (compare Table IV with Table I). This is especially the case for proton functional dependencies which on average improve by approximately 25% with the best (≈30%) and worst (≈10%) improvements provided by the $f_\pi(Z,N) = C_\pi A^\alpha$ and $f_\pi(Z,N) = C_\pi e^{\alpha_\pi \frac{|N-Z|}{N+Z}}$ functional dependencies. The improvements in RMSEs are smaller in the neutron subsystem, with an average improvement over the set of considered functional dependencies being on the level of ≈14%. The best improvements (around 20%) are achieved for the $f_\nu(Z,N) = C_\nu |N-Z|^{\alpha_\nu}$ and $f_\nu(Z,N) = C_\nu e^{\alpha_\nu \frac{|N-Z|}{N+Z}}$ functional dependencies. The exclusion of light nuclei with $Z < 20$ and $N < 20$, which are expected to be significantly affected by beyond mean fields effects, leads to further improvement in the RMSEs (see Table IV) and this effect is especially pronounced in the standard nonlinear least squares fit. One should also note that the restriction to deformed nuclei reduces the impact of outliers. This is seen in the fact that the transition from standard to robust fit does not always reduce RMSEs; this feature is especially pronounced for the set which excludes light nuclei.

Despite all these changes, the general conclusions obtained for the full set of data on scaling factors including different types of nuclei are not affected by the transition to data which

TABLE IV. The parameters of global functional dependencies defined by the fits to the set of "measured+estimated" scaling factors. Note that in this fit only scaling factors defined from deformed nuclei are used. Both the standard (labeled as "Standard fit") and robust (labeled as "Robust fit") nonlinear least squares fits are used here. The results of the fits are presented in the "A/B" format. Here "A" corresponds to the results of the fit to the set of data including all scaling factors of deformed nuclei, while "B" corresponds to the ones which exclude all light nuclei with $Z < 20$ and $N < 20$. Bold style is used for RMSE of the best fit in each group of functional dependencies.

	Standard fit			Robust fit		
	C_i	α_i	RMSE	C_i	α_i	RMSE
1	2	3	4	5	6	7
$f_\pi = C_\pi A^{\alpha_\pi}$	1.801/1.840	−0.0992/−0.1030	**0.0364**/**0.0349**	1.792/1.877	−0.0980/−0.1072	**0.0373**/0.0361
$f_\pi = C_\pi Z^{\alpha_\pi}$	1.646/1.671	−0.0983/−0.1019	0.0392/0.0386	1.642/1.684	−0.0978/−0.1039	0.0409/0.0400
$f_\pi = C_\pi \lvert N-Z\rvert^{\alpha_\pi}$	1.323/1.289	−0.0589/−0.0518	0.0434/0.0355	1.315/1.296	−0.0576/−0.0535	0.0387/0.0356
$f_\pi = C_\pi e^{\alpha_\pi \lvert N-Z\rvert}$	1.201/1.180	−0.0031/−0.0026	0.0434/0.0335	1.187/1.178	−0.00279/−0.0026	0.0379/**0.0348**
$f_\pi = C_\pi e^{\alpha_\pi [\lvert N-Z\rvert/(N+Z)]}$	1.163/1.188	−0.3050/−0.4870	0.0651/0.0459	1.190/1.189	−0.4970/−0.5020	0.0511/0.0473
$f_\nu = C_\nu A^{\alpha_\nu}$	1.465/1.414	−0.0603/−0.0533	0.0531/0.0501	1.482/1.414	−0.0626/−0.0534	0.0531/0.0513
$f_\nu = C_\nu N^{\alpha_\nu}$	1.444/1.410	−0.0644/−0.0592	0.0506/0.0481	1.474/1.421	−0.0688/−0.0608	0.0503/0.0490
$f_\nu = C_\nu \lvert N-Z\rvert^{\alpha_\nu}$	1.283/1.256	−0.0538/−0.0474	**0.0420**/0.0393	1.282/1.264	−0.0535/−0.0495	0.0406/0.0388
$f_\nu = C_\nu e^{\alpha_\nu \lvert N-Z\rvert}$	1.084/1.147	−0.0376/−0.0021	0.0481/0.0425	1.082/1.145	−0.0330/−0.0020	0.0433/0.0417
$f_\nu = C_\nu e^{\alpha_\nu [\lvert N-Z\rvert/(N+Z)]}$	1.084/1.209	−0.0378/−0.673	0.0474/**0.0347**	1.077/1.208	−0.0395/−0.6740	**0.0370**/**0.0352**

are based only on deformed nuclei. In the neutron subsystem, the $f_\nu(Z,N) = C_\nu|N-Z|^{\alpha_\nu}$ and $f_\nu(Z,N) = C_\nu e^{\alpha_\nu \frac{|N-Z|}{N+Z}}$ functional dependencies are still favored over other types of functional dependencies and there is still no way to give a clear preference to one or another. In the proton subsystem, the best description of the data is still provided by two competing functional dependencies of $f_\pi(Z,N) = C_\pi A^\alpha$ and $f_\pi(Z,N) = C_\pi e^{\alpha_\pi \frac{|N-Z|}{N+Z}}$ types, which have different dependence on the isospin.

V. EXTRAPOLATION TO VERY NEUTRON-RICH NUCLEI

It is important to evaluate the evolution of expected uncertainties in the predictions of pairing properties with increasing neutron number N and approaching the neutron drip line. For this purpose we selected the Yb isotope chain in which such evolution has been studied for different classes of CEDFs for constant $f_\pi = f_\nu = 1.075$ in Ref. [89].

Figure 10 compares the variations of neutron and proton scaling factors as a function of neutron number N for different functional dependencies studied in the present paper. For the neutron subsystem, the best RMSEs are provided by $f_\nu(Z,N) = C_\nu e^{\alpha_\nu \frac{|N-Z|}{N+Z}}$ and $f_\nu(Z,N) = C_\nu|N-Z|^{\alpha_\nu}$ functional dependencies (see Tables I, II, and III). However, the preference of one over another depends on whether the standard or robust nonlinear least squares fitting is used and whether light nuclei are excluded from consideration. While neutron scaling factors obtained with these two dependencies are similar (within the accuracy of the present method) for experimentally known nuclei, they differ substantially for very neutron-rich nuclei. The scaling factors defined by the $f_\nu(Z,N) = C_\nu e^{\alpha_\nu \frac{|N-Z|}{N+Z}}$ functional dependence show significant reduction on approaching the neutron drip line, while those based on $f_\nu(Z,N) = C_\nu|N-Z|^{\alpha_\nu}$ reveal smaller decrease. The total reductions of the scaling factors on going on from $N = 78$ to $N = 180$ are 20.2% and 10.7% for these two types of functional dependencies. The functional dependencies of the $f_\nu(Z,N) = C_\nu e^{\alpha_\nu|N-Z|}$, $f_\nu(Z,N) = C_\nu A^{\alpha_\nu}$, and $f_\nu(Z,N) = C_\nu N^{\alpha_\nu}$ types provide less accurate fits (see Tables I, II, and III). In the Yb isotopes, the first one provides scaling factors which are very similar to those obtained by $f_\nu(Z,N) = C_\nu e^{\alpha_\nu \frac{|N-Z|}{N+Z}}$, while the last two deliver neutron scaling factors which only weakly decrease with increasing neutron number and which are close to the constant $f_\nu = 1.075$ used in Ref. [89].

The situation is more complex in the proton subsystem because, in contrast to the neutron one the functional dependencies which include isospin do not get a clear preference over those which depend on mass or proton numbers (see Tables I, II, and III). As a consequence, the two best (in terms of RMSEs) functional dependencies, namely, $f_\pi(Z,N) = C_\pi e^{\alpha_\pi|N-Z|}$ and $f_\pi(Z,N) = C_\pi A^{\alpha_\pi}$ provide drastically different predictions for evolution of proton scaling factors as a function of neutron number [see Fig. 10(b)]. The former one shows drastic decrease of f_π with increasing neutron number, while the latter one is characterized by only modest decrease with an average value close to the constant $f_\pi = 1.075$ used in Ref. [89]. The least accurate functional dependencies given by Eqs. (15) and (17) provide predictions located between these two cases [see Fig. 10(b)]. The $f_\pi(Z,N) = C_\pi Z^{\alpha_\pi}$ functional dependence provides an N-independent f_π value which is close to the $f_\pi = 1.075$ one used in Ref. [89].

Table V shows proton and neutron scaling factors and pairing gaps in the very neutron-rich ^{240}Yb nucleus, located in the vicinity of the two-neutron drip line, calculated with different functional dependencies for scaling factors. In the neutron subsystem, the two best functional dependencies given by $f_\nu(Z,N) = C_\nu|N-Z|^{\alpha_\nu}$ and $f_\nu(Z,N) = C_\nu e^{\alpha_\nu \frac{|N-Z|}{N+Z}}$ provide predictions for neutron scaling factors which differ by ≈8%. This results in neutron pairing gaps which differ by more than 30%. Note, however, that these two functional dependencies predict neutron scaling factors and pairing gaps which

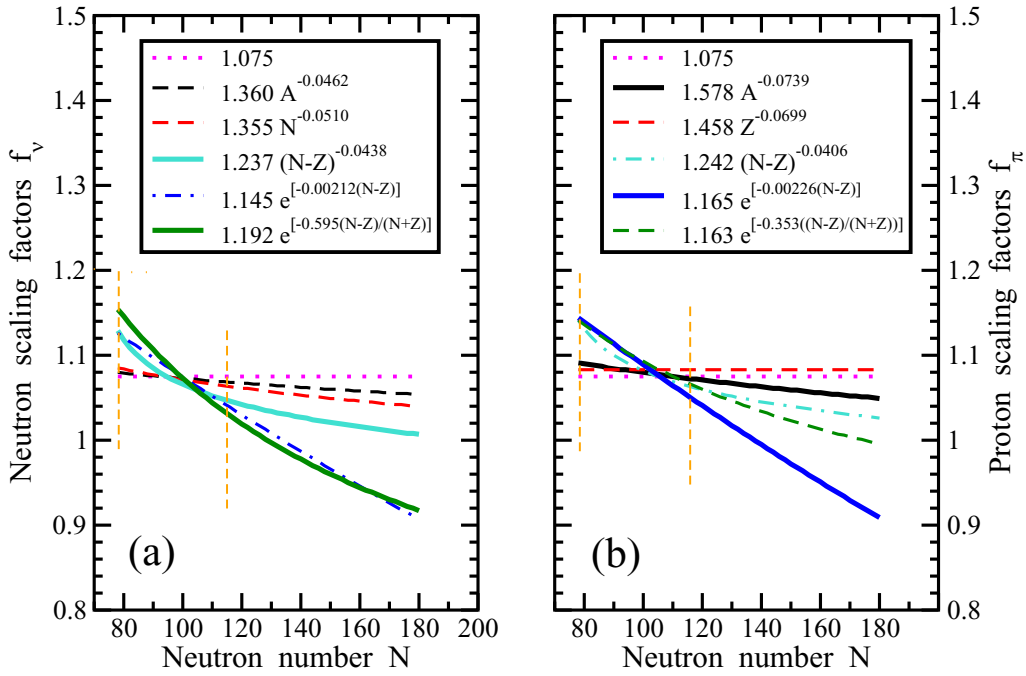

FIG. 10. The variations of neutron and proton scaling factors as a function of neutron number N in the Yb ($Z = 70$) isotopes. Functional dependencies of Eqs. (13)–(17) are given here in inset with the parameters defined in Table III. The pairs of functional dependencies with the best and worst RMSEs are shown by thick solid and thin dashed lines. The dot-dashed thin line is used for the functional dependence located (in terms of RMSE) in between of these pairs. Vertical orange dashed lines are used to indicate the span of neutron numbers for which experimental information on binding energies are available in the Yb isotopes.

are substantially lower than those obtained by functional dependencies with scaling factors dependent either on mass or particle numbers. As discussed above, the situation is more complex in the proton subsystem where our analysis cannot reveal a clear preference for functional dependence of proton scaling factors. This is also seen in Table V which shows that two best dependencies given by $f_\pi(Z,N) = C_\pi e^{\alpha_\pi |N-Z|}$ and $f_\pi(Z,N) = C_\pi A^{\alpha_\pi}$ provide quite drastic differences in the predicted values of proton scaling factors and pairing gaps in ^{170}Yb.

TABLE V. Proton and neutron scaling factors and pairing gaps (Δ^π_{uv} and Δ^ν_{uv}) in the ^{240}Yb nucleus calculated with indicated functional dependencies. The $f_i = \text{const}(Z) = 1.075$ values are scaling factors used for the Yb isotopes in Ref. [89]. The results obtained with two best and two worst (in terms of RMSEs of Table III) functional dependencies for scaling factors are shown by bold and italic values respectively.

1	f_π 2	Δ^π_{uv} 3	f_ν 4	Δ^ν_{uv} 5
$f_i = \text{const}(Z)$	1.075	1.519	1.075	1.373
$f_i = C_i A^{\alpha_i}$	**1.052**	**1.400**	*1.056*	*1.279*
$f_\pi = C_\pi Z^{\alpha_\pi}$ or $f_\nu = C_\nu (N)^{\alpha_\nu}$	*1.083*	*1.567*	*1.042*	*1.215*
$f_i = C_i \lvert N-Z\rvert^{\alpha_i}$	1.030	1.272	**1.011**	**1.042**
$f_i = C_i e^{\alpha_i \lvert N-Z\rvert}$	**0.929**	**0.764**	0.926	0.704
$f_i = C_i e^{\alpha_i [\lvert N-Z\rvert/(N+Z)]}$	*1.004*	*1.155*	**0.930**	**0.720**

These uncertainties in proton and neutron pairing at high isospin could have some impact on the predicted location of the two-neutron drip line (see Ref. [89]) and substantial impact on the heights of fission barriers of neutron-rich nuclei. The latter sensitively depend on the strength of pairing interaction (see Ref. [13]) and the reduction of only neutron pairing at high isospin (similar to the one seen in ^{170}Yb) could increase the static fission barriers by approximately 1 MeV. This could have a significant effect on the r process in actinides and superheavy nuclei (see discussion in Ref. [63]).

VI. CONCLUSIONS

A systematic global investigation of pairing properties based on all available experimental data on pairing indicators has been performed for the first time in the framework of covariant density functional theory. It is based on separable pairing interaction of Ref. [58] and covariant energy density functional NL5(E) [32]. The main results can be summarized as follows:

(1) The optimization of functional dependencies of proton and neutron scaling factors has been performed across the experimentally known nuclear chart. It clearly reveals isospin dependence of neutron pairing with the forms of neutron scaling factors $f_\nu(Z,N) = C_\nu e^{\alpha_\nu \frac{|N-Z|}{N+Z}}$ and $f_\nu(Z,N) = C_\nu |N-Z|^{\alpha_\nu}$ providing the best and comparable descriptions of experimental data. The situation is less clear in the proton subsystem since two best (and comparable in terms of the description of

experimental data) functional dependencies, namely, $f_\pi(Z,N) = C_\pi e^{\alpha_\pi |N-Z|}$ and $f_\pi(Z,N) = C_\pi A^{\alpha_\pi}$, differ drastically with respect of the impact of isospin. The direct comparison of theoretical and experimental pairing indicators extracted from binding energies may help to resolve these uncertainties. However, there is no guarantee that this can be achieved at the mean field level because of potential impact of beyond mean field effects on the binding energies.

(2) The differences in the functional dependencies of scaling factors lead to uncertainties in the prediction of proton and neutron pairing properties which are expected to become especially pronounced at high isospin. They are expected to have some impact on the predicted location of the two-neutron drip line (see Ref. [89]). However, even higher impact is expected on physical observables which extremely sensitively depend on the pairing. These are the moments of inertia of rotational bands (see Refs. [9,10]) and the heights of fission barriers (see Ref. [13]). For example, the reduction of only neutron pairing at high isospin (similar to the one seen in ^{170}Yb) could increase the static fission barriers by approximately 1 MeV and have a significant effect on fission cycling in the *r* process in actinides and superheavy nuclei (see the discussion in Ref. [63]).

(3) Our analysis reveals that in a given part of nuclear chart the scaling factors for spherical nuclei are smaller than those for deformed ones. This result is similar to the ones obtained earlier in nonrelativistic Skyrme and Gogny DFTs (see Refs. [40,47]. Thus, its origin has to be traced back to missing physics which is neglected in all three approaches. The particle-vibration coupling in odd-mass nuclei is the most likely source of such physics. It is well known that it increases the binding energies of odd-*A* nuclei (see Refs. [76,78]) but does not have an impact on binding energies of even-even nuclei. As a consequence, when extracted from experimental binding energies (which by default include PVC effects), the pairing indicators are reduced as compared with those which do not include PVC effects. This effect is especially pronounced in spherical nuclei. Since scaling factors f_v and f_π are fitted to experimental pairing indicators, this leads to a suppression of scaling factors in spherical nuclei as compared with the ones in deformed nuclei.

(4) The present analysis is based on the NL5(E) CEDF which is similar in structure to well known NL3 and NL3* functionals but provides better description of the ground state properties on a global scale [32]. However, it is reasonable to expect that the results about functional dependencies of scaling factors for separable pairing interaction will also be valid for the majority of CEDFs built at the Hartree level, such as those used in global studies of Refs. [36,68,90]. This is due to the fact that all of them have low Lorentz effective masses and thus similar densities of the single-particle states in the vicinity of the Fermi levels as well as similar evolution of these states as a function of particle numbers across the nuclear chart (see Refs. [48,75,87,89]).

The need for optimization of separable pairing interaction of Ref. [58] across the nuclear chart should not be that surprising. First of all, there is no microscopic theory of pairing which would provide the required form and strength of pairing for the CDFT calculations. The discussion on the use of the same interaction in the particle-particle and particle-hole channels is still ongoing but this issue is still dependent on the point of view of the DFT practitioners (see, for example, the discussion in Sec. 2.1 of Ref. [49] and in Sec. 2.1 of Ref. [9]). The common stance in the CDFT and in nonrelativistic Skyrme DFT is that there is no fundamental reason to have the same interaction in both the particle-hole and particle-particle channels because of the use of effective forces. Thus, the Gogny D1S force was adopted in the 1990s for CDFT applications [9,54] and later replaced by the less numerically demanding separable pairing interaction of Ref. [58]. Some differences between the CDFT calculations with the Gogny D1S force in the pairing channel and Gogny DFT calculations are expected, but interestingly enough they are not that significant (see the discussion in Refs. [12,48,70]).

Although the Gogny force is considered as a benchmark for effective pairing forces [49], it is unclear how well this force performs globally even in the Gogny DFT framework when theoretical and experimental pairing indicators extracted from binding energies are confronted. This is because of the absence of such global studies. One should also remember that the calibration of the matrix elements of the Gogny D1S force in the pairing channel has been based on OES in tin isotopes [51] and the description of pairing indicators deviate appreciably from experimental data in some isotopic chains calculated in Ref. [47]. Thus, the Gogny D1S force to which the separable pairing interaction of Ref. [58] has been fitted should in no way be considered as a force optimized in the pairing channel especially in the context of CDFT studies. For example, nonuniqueness of the definition of the pairing channel by different Gogny forces is seen in the calculations of rotational properties of superdeformed bands of the $A \approx 190$ mass region in the CDFT framework [9]. The present approach improves the description of the pairing by separable interaction of Ref. [58] based on the D1S Gogny force by introducing phenomenological isospin and particle/mass dependencies of the strength of this interaction.

ACKNOWLEDGMENT

This material is based upon work supported by the U.S. Department of Energy, Office of Science, Office of Nuclear Physics under Grant No. DE-SC0013037.

[1] A. Bohr and B. R. Mottelson, *Nuclear Structure Volume II: Nuclear Deformation* (W. A. Benjamin, New York, 1975).
[2] V. G. Soloviev, *Theory of Complex Nuclei* (Pergamon, Oxford, 1976).
[3] P. Ring and P. Schuck, *The Nuclear Many-Body Problem* (Springer-Verlag, Berlin, 1980).
[4] A. V. Afanasjev, in *50 Years of Nuclear BCS* (World Scientific, Singapore, 2013), p. 138.
[5] S. Frauendorf and A. Macchiavelli, Prog. Part. Nucl. Phys. **78**, 24 (2014).
[6] Z. Szymański, *Fast Nuclear Rotation* (Clarendon, Oxford, 1983).
[7] W. Satuła, R. Wyss, and P. Magierski, Nucl. Phys. A **578**, 45 (1994).
[8] B. Gall, P. Bonche, J. Dobaczewski, H. Flocard, and P.-H. Heenen, Z. Phys. A **348**, 183 (1994).
[9] A. V. Afanasjev, P. Ring, and J. König, Nucl. Phys. **A676**, 196 (2000).
[10] A. V. Afanasjev and O. Abdurazakov, Phys. Rev. C **88**, 014320 (2013).
[11] A. Valor, J. L. Egido, and L. M. Robledo, Nucl. Phys. A **665**, 46 (2000).
[12] A. V. Afanasjev, J. König, P. Ring, L. M. Robledo, and J. L. Egido, Phys. Rev. C **62**, 054306 (2000).
[13] S. Karatzikos, A. V. Afanasjev, G. A. Lalazissis, and P. Ring, Phys. Lett. B **689**, 72 (2010).
[14] S. E. Agbemava, A. V. Afanasjev, and P. Ring, Phys. Rev. C **93**, 044304 (2016).
[15] *Extended Density Functionals in Nuclear Structure Physics*, Lecture Notes in Physics Vol. 641, edited by G. A. Lalazissis, P. Ring, and D. Vretenar (Springer-Verlag, Heidelberg, 2004).
[16] T. D. Cohen, R. J. Furnstahl, and D. K. Griegel, Phys. Rev. C **45**, 1881 (1992).
[17] W. Koepf and P. Ring, Nucl. Phys. A **493**, 61 (1989).
[18] A. V. Afanasjev and H. Abusara, Phys. Rev. C **81**, 014309 (2010).
[19] U. Hofmann and P. Ring, Phys. Lett. B **214**, 307 (1988).
[20] A. V. Afanasjev and P. Ring, Phys. Rev. C **62**, 031302(R) (2000).
[21] A. V. Afanasjev and H. Abusara, Phys. Rev. C **82**, 034329 (2010).
[22] R. Brockmann and H. Toki, Phys. Rev. Lett. **68**, 3408 (1992).
[23] F. Hofmann, C. M. Keil, and H. Lenske, Phys. Rev. C **64**, 034314 (2001).
[24] M. Serra, T. Otsuka, Y. Akaishi, P. Ring, and S. Hirose, Prog. Theor. Phys. **113**, 1009 (2005).
[25] S. Hirose, M. Serra, P. Ring, T. Otsuka, and Y. Akaishi, Phys. Rev. C **75**, 024301 (2007).
[26] J. E. Drut, R. J. Furnstahl, and L. Platter, Prog. Part. Nucl. Phys. **64**, 120 (2010).
[27] S. Peru and M. Martini, Eur. Phys. J **50**, 88 (2014).
[28] G. A. Lalazissis, T. Nikšić, D. Vretenar, and P. Ring, Phys. Rev. C **71**, 024312 (2005).
[29] T. Nikšić, D. Vretenar, and P. Ring, Phys. Rev. C **78**, 034318 (2008).
[30] X. Roca-Maza, X. Viñas, M. Centelles, P. Ring, and P. Schuck, Phys. Rev. C **84**, 054309 (2011).
[31] P. W. Zhao, Z. P. Li, J. M. Yao, and J. Meng, Phys. Rev. C **82**, 054319 (2010).
[32] S. E. Agbemava, A. V. Afanasjev, and A. Taninah, Phys. Rev. C **99**, 014318 (2019).
[33] D. Vretenar, A. V. Afanasjev, G. A. Lalazissis, and P. Ring, Phys. Rep. **409**, 101 (2005).
[34] J. Meng, H. Toki, S. G. Zhou, S. Q. Zhang, W. H. Long, and L. S. Geng, Prog. Part. Nucl. Phys. **57**, 470 (2006).
[35] T. Nikšić, D. Vretenar, and P. Ring, Prog. Part. Nucl. Phys. **66**, 519 (2011).
[36] S. E. Agbemava, A. V. Afanasjev, D. Ray, and P. Ring, Phys. Rev. C **89**, 054320 (2014).
[37] *Relativistic Density Functional for Nuclear Structure*, International Review of Nuclear Physics Vol. 10 edited by J. Meng (World Scientific, Singapore, 2016).
[38] W. Satula, J. Dobaczewski, and W. Nazarewicz, Phys. Rev. Lett. **81**, 3599 (1998).
[39] M. Bender, K. Rutz, P.-G. Reinhard, and J. A. Maruhn, Eur. Phys. J. A **8**, 59 (2000).
[40] G. F. Bertsch, C. A. Bertulani, W. Nazarewicz, N. Schunck, and M. V. Stoitsov, Phys. Rev. C **79**, 034306 (2009).
[41] T. Duguet, P. Bonche, P.-H. Heenen, and J. Meyer, Phys. Rev. C **65**, 014310 (2001).
[42] A. Mukherjee, Y. Alhassid, and G. F. Bertsch, Phys. Rev. C **83**, 014319 (2011).
[43] C. A. Bertulani, H. Liu, and H. Sagawa, Phys. Rev. C **85**, 014321 (2012).
[44] M. Yamagami, J. Margueron, H. Sagawa, and K. Hagino, Phys. Rev. C **86**, 034333 (2012).
[45] S. Changizi, C. Qi, and R. Wyss, Nucl. Phys. A **940**, 210 (2015).
[46] S. Hilaire, J.-F. Berger, M. Girod, W. Satula, and P. Schuck, Phys. Lett. B **531**, 61 (2002).
[47] L. M. Robledo, R. Bernard, and G. F. Bertsch, Phys. Rev. C **86**, 064313 (2012).
[48] J. Dobaczewski, A. V. Afanasjev, M. Bender, L. M. Robledo, and Y. Shi, Nucl. Phys. A **944**, 388 (2015).
[49] L. M. Robledo, T. R. Rodríguez, and R. R. Rodríguez-Guzmán, J. Phys. G **46**, 013001 (2019).
[50] A. K. Kerman, Ann. Phys. (NY) **12**, 300 (1961).
[51] D. Gogny, in *Nuclear Self-Consistent Fields, Proceedings of the International Conference*, Center for Theoretical Physics, Trieste, Italy, 1975, edited by G. Ripka and M. Porneuf (North-Holland, Amsterdam, 1975), p. 333.
[52] J. F. Berger, M. Girod, and D. Gogny, Nucl. Phys. A **428**, 23 (1984).
[53] J. F. Berger, M. Girod, and D. Gogny, Comput. Phys. Commun. **63**, 365 (1991).
[54] T. Gonzalez-Llarena, J. L. Egido, G. A. Lalazissis, and P. Ring, Phys. Lett. B **379**, 13 (1996).
[55] A. V. Afanasjev, Phys. Scr. **89**, 054001 (2014).
[56] G. A. Lalazissis, D. Vretenar, and P. Ring, Nucl. Phys. A **679**, 481 (2001).
[57] M. Serra and P. Ring, Phys. Rev. C **65**, 064324 (2002).
[58] Y. Tian, Z. Y. Ma, and P. Ring, Phys. Lett. B **676**, 44 (2009).
[59] Y. Tian, Z. Y. Ma, and P. Ring, Phys. Rev. C **80**, 024313 (2009).
[60] T. Nikšić, P. Ring, D. Vretenar, Y. Tian, and Z. Y. Ma, Phys. Rev. C **81**, 054318 (2010).
[61] S. E. Agbemava, A. V. Afanasjev, D. Ray, and P. Ring, Phys. Rev. C **95**, 054324 (2017).
[62] J. Zhao, B.-N. Lu, D. Vretenar, E.-G. Zhao, and S.-G. Zhou, Phys. Rev. C **91**, 014321 (2015).
[63] A. Taninah, S. E. Agbemava, and A. V. Afanasjev, Phys. Rev. C **102**, 054330 (2020).
[64] Y. K. Wang, Phys. Rev. C **96**, 054324 (2017).

[65] B. W. Xiong, Phys. Rev. C **101**, 054305 (2020).
[66] Y. Tian, Z. Y. Ma, and P. Ring, Phys. Rev. C **79**, 064301 (2009).
[67] V. Prassa, T. Nikšić, G. A. Lalazissis, and D. Vretenar, Phys. Rev. C **86**, 024317 (2012).
[68] K. Q. Lu, Z. X. Li, Z. P. Li, J. M. Yao, and J. Meng, Phys. Rev. C **91**, 027304 (2015).
[69] Z. Shi, A. V. Afanasjev, Z. P. Li, and J. Meng, Phys. Rev. C **99**, 064316 (2019).
[70] A. V. Afanasjev, T. L. Khoo, S. Frauendorf, G. A. Lalazissis, and I. Ahmad, Phys. Rev. C **67**, 024309 (2003).
[71] L. J. Wang, B. Y. Sun, J. M. Dong, and W. H. Long, Phys. Rev. C **87**, 054331 (2013).
[72] W. J. Huang, G. Audi, M. Wang, F. G. Kondev, S. Naimi, and X. Xu, Chin. Phys. C **41**, 030002 (2017).
[73] K. J. Pototzky, J. Erler, P.-G. Reinhard, and V. O. Nesterenko, Eur. Phys. J. A **46**, 299 (2010).
[74] L. Bonneau, P. Quentin, and P. Möller, Phys. Rev. C **76**, 024320 (2007).
[75] A. V. Afanasjev and S. Shawaqfeh, Phys. Lett. B **706**, 177 (2011).
[76] E. V. Litvinova and A. V. Afanasjev, Phys. Rev. C **84**, 014305 (2011).
[77] A. V. Afanasjev and E. Litvinova, Phys. Rev. C **92**, 044317 (2015).
[78] J. Dechargé and D. Gogny, Phys. Rev. C **21**, 1568 (1980).
[79] F. A. Gareev, S. P. Ivanova, V. G. Soloviev, and S. I. Fedotov, Phys. Elem. Part. At. Nucl. **4**, 357 (1973).
[80] B. A. Alikov, K. N. Badalov, V. O. Nesterenko, A. V. Sushkov, and J. Wawryszczuk, Z. Phys. A **331**, 265 (1988).
[81] N. Y. Shirikova, A. V. Sushkov, L. A. Malov, and R. V. Jolos, Eur. Phys. J. A **51**, 21 (2015).
[82] K. Neergård and I. Bentley, Phys. Rev. C **99**, 054315 (2019).
[83] G. A. Lalazissis, J. König, and P. Ring, Phys. Rev. C **55**, 540 (1997).
[84] G. A. Lalazissis, S. Karatzikos, R. Fossion, D. P. Arteaga, A. V. Afanasjev, and P. Ring, Phys. Lett. B **671**, 36 (2009).
[85] W. Koepf and P. Ring, Nucl. Phys. A **511**, 279 (1990).
[86] K. Rutz, M. Bender, P.-G. Reinhard, and J. A. Maruhn, Phys. Lett. B **468**, 1 (1999).
[87] S. E. Agbemava, A. V. Afanasjev, T. Nakatsukasa, and P. Ring, Phys. Rev. C **92**, 054310 (2015).
[88] P. Möller and J. Nix, Nucl. Phys. A **536**, 20 (1992).
[89] A. V. Afanasjev, S. E. Agbemava, D. Ray, and P. Ring, Phys. Rev. C **91**, 014324 (2015).
[90] L. Geng, H. Toki, and J. Meng, Prog. Theor. Phys. **113**, 785 (2005).